Carbohydrate Polymers 364 (2025) 123778

Contents lists available at ScienceDirect

Carbohydrate Polymers

journal homepage: www.elsevier.com/locate/carbpol

Silylation of wheat straw cellulose pulp for its valorization as rheology modifier of industrial hydrophobic fluids: Cases of castor oil and bitumen

M. Trejo-Cáceres, J.E. Martín-Alfonso *, J.M. Franco

Chemical Product and Process Technology Research Center (Pro²TecS), Department of Chemical Engineering and Materials Science, ETSI, University of Huelva, 21071 Huelva, Spain

ARTICLE INFO

Keywords:
Cellulose pulp
Functional materials
Silylation
Rheology
Tribology
Product engineering

ABSTRACT

This work explores an innovative approach to developing novel oleo- and bitumen-based dispersions, which are potentially applicable as semisolid lubricants and bitumen binders, respectively, using lignocellulosic biomass. In particular, it focuses on investigating the impact of the silylation process of wheat straw Kraft cellulose pulp (KWP) on the rheological properties of these dispersions. To this end, KWP was functionalized with *tert*-butyldimethylsilyl chloride (TBDMSCl), using imidazole (ImH) as a catalyst, through a simple and efficient method. Different conditions of the silylation process such as temperature (20–100 °C), TBDMSCl/ImH ratio (1/2.5–2.5/2.5), and silylation time (2–24 h) were applied to illustrate the flexibility of the proposed methodology. Modified pulps with oil and/or bitumen structuring ability were obtained, as a result of the interaction between the hydrophobic alkyl-siloxane segment-containing fibers and these hydrophobic fluids, which enhance the compatibility between both components. Oleo-dispersions with a similar viscoelastic response to lithium grease, used as a benchmark, exhibited significantly reduced coefficients of friction and wear. Meanwhile, bitumen-dispersions displayed a substantial improvement in stiffness and elasticity with the temperature. This work may offer a novel strategy for developing rheology modifiers or structuring agents for industrial hydrophobic fluids.

1. Introduction

In recent years, there has been considerable interest in using and evaluating agro-industrial materials to produce value-added products with multifunctional properties with the aim of reducing the problems associated with the use of fossil raw materials, such as increased carbon footprint, global warming, ozone depletion, and waste generation as a non-biodegradable resource (Abdelwahab et al., 2021). In connection with this, both the lubricant and bitumen industries are actively exploring the use of renewable materials to develop eco-friendly semisolid lubricants or bitumen binders. This includes the development of thickener or additives that meet the performance requirements of traditional metallic soaps and synthetic 'passive' or 'active' polymers. The aim is to create products that are as effective as their traditional counterparts, but with a reduced environmental impact. Among renewable materials, biomass-derived materials have increasingly significant potential in the fields of lubricants and asphalt pavement (Elshorbagy et al., 2019; J. E. Martín-Alfonso et al., 2020; Zhou et al., 2021). Approximately 950 million tons of lignocellulosic biomass is produced annually by the agricultural sector in Europe (Saleem, 2022). Various types of natural fibers derived from lignocellulosic biomass, such as eucalyptus, sisal, and pinus, have been used as additives in bitumen as a common strategy to control the bitumen's degradation in gap-graded and open-graded asphalt mixtures (Desseaux et al., 2018; Eskandarsefat et al., 2019). These lignocellulosic materials have also been tested as potential thickeners for vegetable oils (Cortés-Triviño et al., 2019; J. E. Martín-Alfonso et al., 2018). In the development of these products, cellulose fibers may have some advantages over other commonly used non-renewable materials. This is because of their abundance, biodegradability, facile modification of surface chemistry and unique physical, chemical and mechanical properties (Wei et al., 2020). At appropriate concentrations, cellulose fibers and cellulose nanocrystals can form highly viscous suspensions in aqueous medium due to the occurrence of percolation networks and chemical interactions as well as entanglement. Under continuous shearing, cellulose fibers or cellulose nanocrystals orient along the flow direction, producing a complex shear thinning behavior with several regions viscosity profile. At rest, cellulose fibers or cellulose nanocrystals recover much of their initial structure in a short time, allowing rapid recovery of steady-state viscosity and viscoelastic properties (Shafiei-Sabet et al., 2012). These

* Corresponding author.
E-mail address: jose.martin@diq.uhu.es (J.E. Martín-Alfonso).

https://doi.org/10.1016/j.carbpol.2025.123778
Received 10 February 2025; Received in revised form 15 May 2025; Accepted 18 May 2025
Available online 20 May 2025

attractive flow features allow cellulose fibers and cellulose nanocrystals to serve as effective rheological modifiers in a wide range of applications such as 3D printing inks, oilfield and construction materials, food additives, coatings and cosmetics /personal care products and so on (Li et al., 2021). Thus, a number of scientific and technical studies have recently been conducted to investigate the complex rheological properties of aqueous cellulose fibers and cellulose nanocrystals (Shafiei-Sabet et al., 2016; Yuan et al., 2021). However, cellulose pulp in its native form is hydrophilic due to the numerous hydroxyl groups present in the cellulose, hemicellulose, and lignin structure. This results in poor compatibility of the pulp with hydrophobic fluids, thus limiting its use as a rheology modifier or structuring agent of these fluids.

An adequate chemical and physical compatibility of the pulp in the fluids is an important factor in defining appropriate rheological and functional properties of a dispersion. Therefore, many attempts have been made to modify the pulp fibers to obtain hydrophobically "modified" pulp by using the available hydroxyl groups in its structure for chemical modification (Adenekan & Hutton-Prager, 2019; Arancibia et al., 2021; Bendahou et al., 2015; Lee et al., 2020; Trejo-Cáceres et al., 2024; Tursi et al., 2018). The silylation reaction is a particularly attractive way of modifying the functional properties of pulp fibers, as it is effective in increasing the interaction of the treated fibers with non-polar media and can therefore significantly broaden their range of applications (Sayadi & Brouillette, 2024). Furthermore, chemical modification by silylation procedure is relatively cheap since silylation agents are effective and not costly. The principle of silylation is to replace the hydroxyl groups of the fibers with alkylsilyl groups, which have a more hydrophobic nature. The presence of these compounds on pulp fibers provides unique features such as improved mechanical and physicochemical properties, as well as good adhesion (Z. Zhang et al., 2015). The silylation using organic silicon compounds, such as alkoxysilanes, to study the tailoring properties of cellulose fibers has been previously reported. Qu et al. (Qu et al., 2012) utilized 3-methacryloxypropyl-trimethoxysilane to enhance the surface of cellulose nanofibers and improve their interfacial adhesion with poly(lactic acid). Similarly, Frone et al. (Frone et al., 2013) demonstrated improved dispersion of cellulose nanofibers modified with 3-amino-propyltriethoxysilane in the poly(lactic acid) matrix compared to untreated fibers. Whereas, Lu et al. (Lu et al., 2008) modified the surface character of microfibrillated cellulose from hydrophilic to hydrophobic using 3-glycidox-ypropyltrimethoxysilane to improve the adhesion between the fibers and an epoxy polymer matrix. However, we are not aware of any previous attempts to use silylation reaction to design novel oleo−/bitumen-dispersions potentially applicable as semisolid lubricants and bitumen binders from lignocellulosic sources, which could gain significant attention due to their numerous applicable opportunities. In particular, the main objective of this work was to study the impact of the silylation process of wheat straw Kraft cellulose pulp on the rheological and tribological properties of dispersions based on two of the most important non-polar fluids (bitumen and oil). Taking this into account, the hypothesis of this work is that the physicochemical properties of wheat straw fibers are significantly influenced by the silylation process, which will allow to improve the physical interaction with oil and bitumen, and the preparation and optimization of semisolid lubricant and bitumen binder formulations. In addition, this approach will provide opportunities for the valorization of wheat straw pulp to create high added-value functional products. Wheat straw as lignocellulosic biomass from agricultural feedstock is one of the abundantly available renewable sources, which is usually abandoned and burned every year, causing environmental problems (Bangar et al., 2023). Initially, pulp fibers were produced using the kraft pulping alkaline process. Subsequently, wheat straw pulp was reacted with *tert*-butyldimethylsilyl chloride in the presence of *N*,*N*-dimethylformamide and imidazole as a catalyst. This part of the study aimed to investigate the influence of key reaction parameters, such as temperature, imidazole/KWP mass ratio, and reaction time, on the chemical, morphological, and thermal properties of the silylated pulp. The specific goal was to obtain a variety of samples with different physicochemical properties. Finally, the silylated wheat straw pulps were evaluated as potential rheology modifiers or structuring agents for developing sustainable semisolid lubricants and bitumen binders as an ecological alternative of fossil fuel-based products.

2. Materials and methods

2.1. Materials

Wheat straw was donated by local farmers (Huelva region, Andalusia, Spain). Tert-butyldimethylsilyl chloride (TBDMSCl), imidazole (ImH), dimethylformamide (DMF, purity ≥99.8 %), methanol (CH_3OH, purity ≥99.9 %), hexane (C_6H_{14}, purity ≥99.0 %), tetrahydrofuran (THF, purity ≥99.0 %), sulfuric acid (H_2SO_4 ≥ 99.9), sodium hydroxide (NaOH) and sodium sulfide (Na_2S) were purchased from Merck Sigma-Aldrich and used as received. Chemicals used for silylation were analytical reagents and solutions were prepared with distilled water. Bitumen (Eiffage, Spain) and castor oil (Guinama, Spain) were used as non-polar fluids. Table S1 shows some relevant physicochemical properties and other general information of the castor oil and bitumen. Furthermore, a commercial multipurpose lithium lubricating grease (Bellota, Spain) was used as a benchmark.

2.2. Pulping process

Wheat straw was subjected to a Kraft digestion at 160 °C, for 60 min, using 17 wt% NaOH solution and 28 wt% Na_2S solution (on dry matter, o.d.m) at a liquid/solid ratio of 10 L/1 kg in a 15 L batch reactor heated by an outer jacket heater and stirred by rotating the reaction vessel with a motor. After the pulping process, the cellulose pulp was washed to remove the reagent and soluble substances to obtain the final cellulose pulp (KWP).

The carbohydrate composition of the raw material and kraft wheat straw pulp was determined by hydrolysis according to Theander and Westerlund method (Theander & Westerlund, 1986) and the monosaccharides were determined by using high performance liquid chromatography (HPLC). Further, the lignin content was determined according to the standard method (TAPPI T222 om-12), and the mass of the solvent extracted samples was calculated according to TAPPI T207 cm-08. In summary, the sample was subjected to hydrolysis at 30 °C with 5 mL of 72 wt% H_2SO_4 for 1 h and quantitative post-hydrolysis with 4 wt% H_2SO_4 (adding water until 148.67 g) at 121 °C for 60 min in an autoclave vessel. Prior to HPLC analysis, the solid residue from the post-hydrolysis process was recovered by filtration and considered to be Klason lignin. The hydrolysates were chemically analyzed following the TAPPI T249-em-09 method. The acid hydrolysis liquor was used to determine the monomeric sugars (xylose, arabinose, and glucose) and acetyl groups. An Aminex HPX-87H ion-exchange column was used as the stationary phase at 30 °C, and 0.05 M H_2SO_4 was used as the mobile phase at a flow rate of 6 mL/min. The monosaccharide contents were expressed in terms of glucan, xylan, and arabinan. Table 1 displays the chemical composition of the of raw kraft wheat straw and pulp. It is evident that the cellulose content increased significantly after the alkali pulping process, as other components such as hemicelluloses (xylan + arabinan) and lignin decreased with respect to glucan content. On the

Table 1
Chemical composition of raw kraft wheat straw and derived cellulose pulp.

Chemical component	Wheat straw (wt%)	Wheat straw cellulose pulp (wt%)
Glucan	32.8 ± 1.70	74.8 ± 2.01
Xylan	14.6 ± 1.10	17.9 ± 0.91
Arabinan	2.02 ± 0.19	1.20 ± 0.15
Klason lignin	18.6 ± 0.96	2.90 ± 0.11
Extractive	22.1 ± 1.37	3.20 ± 0.27

other hand, Table S2 shows the physical dimensions of wheat straw Kraft cellulose pulp.

2.3. Silylation of wheat straw pulp

The silylation of KWP was conducted in DMF using TBDMSCl as the silylation reagent and imidazole as the catalyst. The reaction was carried out in a round-bottomed flask that was immersed in an oil bath for temperature control, with continuous magnetic stirring. In brief, 1 g of KWP and 15 ml DMF were mixed in a 100 mL flask and the amount of TBDMSCl required was added together with the imidazole by varying temperature (20, 30, 40, 60, 80, 100 °C), TBDMSCl/ImH ratio (1:2.5, 1.5:2.5, 2:2.5, 2.5:2.5) and reaction time (2, 3, 4, 6, 12, 24 h). The imidazole/KWP mass ratio was chosen based on previous studies by Lv et al. (Lv et al., 2019) and Patschinski et al. (Patschinski & Zipse, 2015) to ensure sufficient imidazole as an auxiliary base to neutralize the HCl formed during the reaction and to ensure completion of the reaction. The reaction mixture was then stirred at controlled temperature. Finally, after filtration under vacuum, a mixture of THF and methanol (80:20) was added under stirring to dissolve the imidazole chloride formed. After filtration, the product was washed twice with 100 mL of THF to dissolve any possible by-products and reactants without consumption (Goussé et al., 2004). The final filtered product was washed with 100 mL of n-hexane to remove solvents such as DMF and THF. The silylated pulp was dried in a vacuum oven at 50 °C for 24 h. Each experiment was performed three times to ensure the repeatability of the results.

2.4. Characterization of silylated pulps

2.4.1. Fourier transform infrared spectroscopy (FTIR) analysis

FTIR spectroscopy analyses were carried out to determine changes in the chemical composition and functional groups due to silylation. The samples were mixed to 1 wt% with KBr, ground into powder using a mortar and pestle and then pressed into tablets. The spectra of samples were obtained in a JASCO FT/IR- 4200 spectrometer. Each sample was scanned 25 times at a resolution of 4 cm^{-1} over the wavenumber region of 4000–400 cm^{-1}.

2.4.2. NMR spectroscopy

Proton and carbon nuclear magnetic resonance (^{1}H NMR and ^{13}C NMR) spectra of the samples dissolved in DMSO-d6 were measured on an Avance III 600 NMR spectrometer (Bruker, Germany) equipped with a Larmor frequency of 600 MHz using a Bruker 4 mm N-P/H MAS probe, spun at a MAS frequency of 14 kHz. The ^{1}H spectra were recorded at 600 MHz using 24 scans and a sweep width of 4504.5 Hz. The ^{13}C spectra were observed at 75.5 MHz using 10,000 scans and a sweep width of 14 kHz. Chemical shifts were expressed as parts per million (ppm) relative to internal DSS: $\delta = 0$ ppm for ^{1}H and $\delta = 0$ ppm for ^{13}C.

2.4.3. X-ray photoelectron spectroscopy (XPS)

X-ray photoelectron spectroscopy (XPS) characterization technique was performed using an Axis Ultra DLD electron spectrometer (Kratos, UK) to investigate the chemical composition present on the samples surface. The spectra were collected with a monochromate Al-Kα radiation (1486.6 eV) operating at 150 W. The base pressure of the sample analysis chamber was ≈1.33×10^{7} Pa (or 1.0×10^{9} Torr), and the film specimens had a dimension of 3 square millimeters. The atomic concentration of carbon (C), oxygen (O) and silicon (Si) was determined from the survey spectra, (0–1300 eV range, 80 eV pass energy, 0.5 eV step size). While the high-resolution spectra were recorded in 0.1 eV step size with 20 eV analyzer pass energy. All XPS data analysis was completed using the CasaXPS software package.

2.4.4. Induction coupling plasma-optical emission spectrometry (ICP-OES)

The concentration of silicon from silylated samples was determined by induction coupling plasma-mass spectrometry according to Goussé et al. (Goussé et al., 2002) using an Agilent 7700× spectrometer (Agilent Technologies Inc., USA). Fifty milligrams of silylated samples and 1 mL H_2SO_4 were mixed in a Pt crucible, which was heated to 180 °C until no more smoke was produced (~ 48 h). The crucible was placed in an oven at 700 °C for 2 h, and a molten mixture of K_2CO_3/Na_2CO_3 (1/1) was added to the white ashes. This mixture was heated to 600 °C for 30 min. After cooling to room temperature, a known amount of water was added to yield aqueous solutions that were analyzed by induction coupling plasma-optical emission spectrometry (ICP-OES).

2.4.5. X-ray diffraction (XRD) analysis

X-ray diffraction (XRD) patterns of samples were obtained on a D8 Advance X-ray diffractometer (Bruker, Germany) with nickel-filtered ($V = 40$ kV, $I = 30$ mA) CuKα radiation as the X-ray source ($\lambda = 1.5418$ Å). The scanning rate was 3.6 s per step with a scanning step of 0.02° to reduce the noise in the peaks. The range of 2θ scan was 5 to 45° (2θ). The crystallinity index (CI) was calculated according to Segal et al. method (Segal et al., 1959):

$$CI(\%) = \left(\frac{I_{200}\text{-}I_{am}}{I_{200}}\right) \times 100 \quad (1)$$

where I_{200} was the maximum intensity of the 200 peak ($2\theta = 22.7°$), and I_{am} was the minimum intensity which represents the intensity of the data at $2\theta = 18–19°$ between the 1–10/110 (15.7°) and 200 (22.4°) peaks (French, 2014).

2.4.6. Contact angle measurements

Sessile-drop contact angle measurements to evaluate the hydrophobicity of the samples were carried out using a dynamic goniometer, by monitoring the speeding of a water drop laying on the surface of the KWP and silylated samples. Apparent dynamic contact angles were obtained by capturing side-images of the drop as a function of time using a CCD camera (PixeLink PL-A741) and analyzing the shape of its profile. A droplet of deionized water (~5 μL) was deposited onto the surface of a sample film at room temperature (~ 23 °C) and the water spread was measured using the axisymmetric drop shape analysis profile (ADSA-P). To prepare the films, the samples were pressed for 30 s at 1000 kPa using a manual hydraulic press. OpenDrop v3.3.2 software was used to analyze images and measure the contact angles.

2.4.7. Scanning electron microscopy (SEM) observations

The morphological characteristics of neat KWP and silylated samples were observed by means of scanning electron microscopy in a FlexSEM 1000 II microscopy, after sputtering the samples with a gold under vacuum, operating at 10 kV acceleration voltage and 5 mm working distance.

2.4.8. Thermogravimetric analysis (TGA)

The thermal stability of samples was analyzed using a thermogravimetric analyzer Q-50 (TA Instruments, USA). Approximately, 5–6 mg of each sample were placed on a Pt pan under N_2 gas flow of 100 mL/min and heated from 30 °C to 600 °C at 10 °C/min.

2.5. Manufacture of oleo−/bitumen-dispersions

Oleo-dispersions were prepared by adding the silylated KWP to the castor oil in an open vessel, using a RW-20 mixer (IKA, Germany) coupled with a helical ribbon impeller geometry at room temperature (~ 23 °C), and a rotation speed of 60 rpm for 1 h. Pulp concentration in the oleo-dispersion was in the range of 5–12.5 wt%. A homogenization treatment (rotational speed: 8800 rpm) was applied afterwards for 5 min using a rotor–stator turbine (Ultra Turrax T-50, Ika). The oleo-dispersions were then stored at room temperature. Bitumen dispersions were similarly prepared in an open vessel, using the RW-20 mixer (IKA, Germany) equipped with a helical ribbon impeller. The dispersions

were processed for 1 h, at 170 °C and a stirring speed of 200 rpm at a total pulp concentration of 4 wt%. The bitumen dispersions were placed on a sheet of aluminum foil and stored in a freezer (~ −18 °C) immediately after preparation to avoid modification of the pulp-bitumen phase.

2.6. Rheological characterization

The rheological characterization of silylated KWP dispersions was performed in a controlled-stress rheometer Physica MCR-301 (Anton Paar, Austria), using a roughened plate–plate geometry (25 mm diameter and 1 mm gap) for oleo-dispersions to avoid possible slip phenomena and a coaxial cylinder geometry (height: 40 mm, inner diameter: 27 mm, outer diameter: 29 mm) for bitumen-dispersions. For the oleo-dispersions, frequency sweep tests were performed in the range of 0.03 and 100 rad/s, within the linear viscoelastic region, as well as viscous flow tests, at shear rates from 0.01 to 100 s^{-1} at 23 °C. Bitumen-dispersions were characterized by temperature sweep tests in oscillatory shear, at a heating rate of 1 °C/min, a constant frequency of 10 rad/s, and 1 % strain within the linear viscoelastic region. Steady-state viscous flow tests were also performed at 135 and 165 °C, in a shear rate range of 10^{-2} to 10^{2} s^{-1}.

2.7. Microstructural characterization of oleo-dispersions

The microstructure of the oleo-dispersions was analyzed using an AURIGA (Zeiss, USA) scanning electron microscope, with a secondary electron detector at an acceleration voltage of 20 kV. A double fixation protocol with 2.5 % glutaraldehyde in 0.1 M cacodylate buffer for 2 h, and 1 % osmium tetroxide for 1 h was applied, followed by a critical point drying treatment (Pathan et al., 2010). Finally, the samples were sputtered with a very thin layer of gold to improve the quality of the micrographs.

2.8. Tribological characterization of oleo-dispersions

The tribological tests of the oleo-dispersions were carried out using a T-PTD 200 tribology cell in a rotating ball-on-three-plates configuration connected to a Physica MCR-501 rheometer. In this configuration, a ball ($r = 0.635$ cm) of stainless steel X5CrNi18–10 (1.4301) was rotated in contact with three plates of the same stainless steel. The three plates were fixed at an angle of 45° to the loading axis. The plate holder was suspended horizontally so that the loading axis and the centre of the three plates could be self-aligned when a normal load was applied. The schematic illustration of the testing configuration can be found elsewhere (J. E. Martín-Alfonso & Valencia, 2015). The friction coefficient was monitored over 10 min at 23 °C by applying a normal force of 20 N, resulting in a maximum contact Hertzian pressure of ~1.63 GPa, and setting a constant rotational speed of 20 rpm. Resulting wear scars on the steel plates were examined using a scanning electronic microscope.

2.9. Statistical analysis

All measurements were determined in triplicate and the results were recorded as the mean ± standard deviation. The analysis of the experiments was conducted with the OriginLab statistical software (version 9.0) based on regression analysis of the experimental data. Analysis of variance (ANOVA) was used for statistical evaluation where $p < 0.05$ was stablished as statistically significant.

3. Results and discussion

3.1. Influence of silylation on the chemical, morphological and thermal properties of kraft wheat straw pulp

The silylation reaction of wheat cellulose pulp was carried out following Corey's procedure. This is a common method for transforming primary and secondary alcohols to sugars (Corey & Kim, 1972), and is particularly useful for protecting 1,2- and 1,3-diols. In this case, *tert*-butyldimethylsilyl chloride (TBDMSCl) was used as the silylating reagent, *N*,*N*-dimethylformamide (DMF) as the solvent, Lewis base, and catalyst, and imidazole as auxiliary base and catalyst (Lawandi et al., 2016; Patschinski et al., 2014). The selection of reagents is crucial for achieving both high efficiency and selectivity in the reaction. Both imidazole and DMF have been shown to be effective catalysts for the silylation of alcohols, resulting in high regioselectivity at the 6-position of the glucopyranoside ring (Lv et al., 2019). Fig. 1 displays the two silylation mechanisms occurring in parallel: one catalysed by imidazole (Fig. 1a) and the other by DMF (Fig. 1b). In the first, imidazole initially forms a highly electrophilic and reactive counterion (silyl imidazole), which then reacts with the hydroxyl groups of cellulose and activates silylation. As the catalyst remains unreacted after the process and forms a highly stable hydrochloride salt with the chlorides released during the reaction, its recycling is very difficult (Lv et al., 2019; Patschinski & Zipse, 2015). Due to the high reactivity of the silyl imidazole, substitution occurs mostly at the primary alcohol (6-position) (Lawandi et al., 2016). Additionally, substitution occurs at the secondary alcohols at positions 2 and 3, resulting in disubstituted products. This disubstituted products are predominantly composed of 72 % of the isomer 2,6-bis-TBDMS cellulose ether and 28 % of the isomer 3,6-bis-TBDMS cellulose ether due to intramolecular transpositions resulting from the reactivities of the reagents and the reaction temperature (Dimakos & Taylor, 2018; Lawandi et al., 2016). Fig. 1b illustrates the process of DMF catalysis. DMF reacts with TBDMSCl to form a transient catalytic cycle intermediate (silylated DMF) (Patschinski & Zipse, 2015), which then reacts with the hydroxyl groups of cellulose. This reaction predominantly yields the monosylated product at C_6 with 100 % regioselectivity due to the low reactivity of the transient complex and the steric hindrance of the primary alcohols in cellulose. This complex can also give rise to other inactive silylation products for cellulose silylation, such as *tert*-butyldimethylsiloxane (TBDMSO) and *tert*-butylhydroxydimethylsiloxane (TBDMSOH). These side reactions occur due to long reaction times and high temperatures, and traces of water in the solvent, respectively. As a result, conversions may be lower than the expected (Lv et al., 2019).

Fig. 2. displays the FTIR spectra of the neat KWP and silylated samples at a temperature of 40 °C and a TBDMSCl/imidazole ratio of 1.5/2.5 as a function of reaction time. The wheat straw pulp exhibits an absorption broad peak at 3670–3000 cm^{-1}, which is associated with the stretching vibrations of the hydroxyl group (OH) of cellulose. The mixture of inter- and intramolecular hydrogen bonds is considered to cause the broadening of the OH band (Popescu et al., 2011). Additionally, the peak at 2912 cm^{-1} corresponds to the stretching vibration of C—H groups in CH_2. The peak located at 1646 cm^{-1} correspond to the vibration of water molecules absorbed in cellulose (Carrillo et al., 2004). The interval between 1500 and 1200 cm^{-1} pertains to CH_2 symmetric bending, CH bending, and CH_2 wagging vibration, respectively (Popescu et al., 2011). In the region below 1200 cm^{-1} bands at 1164, 1111, 1054, 1032, and 897 cm^{-1} can be observed, which are attributed to the asymmetric C–O–C bridge stretching, the anhydroglucose ring asymmetric stretching, C—O stretching, C—H in-plane deformation, and C—H deformation of cellulose, respectively (Åkerholm et al., 2004; H. Chen et al., 2010). The band at around 1430 cm^{-1} could be associated with the amount of the crystalline structure of the cellulose, while the band at 897 cm^{-1} is assigned to the amorphous region in cellulose (Åkerholm et al., 2004). The KWP pulp has a low lignin content (see Table 1). Consequently, the fingerprint region from 600 to 1500 cm^{-1} is primarily associated with cellulose and hemicelluloses, and only a few characteristic bands of lignin, such as those at 1513 and 1741 cm^{-1}, can be observed (Z. Chen, Hu, et al., 2015). The spectra of silylated samples confirm the silylation of wheat straw pulp. This is supported by the presence of the characteristic bands of silane identified at 1257 cm^{-1},

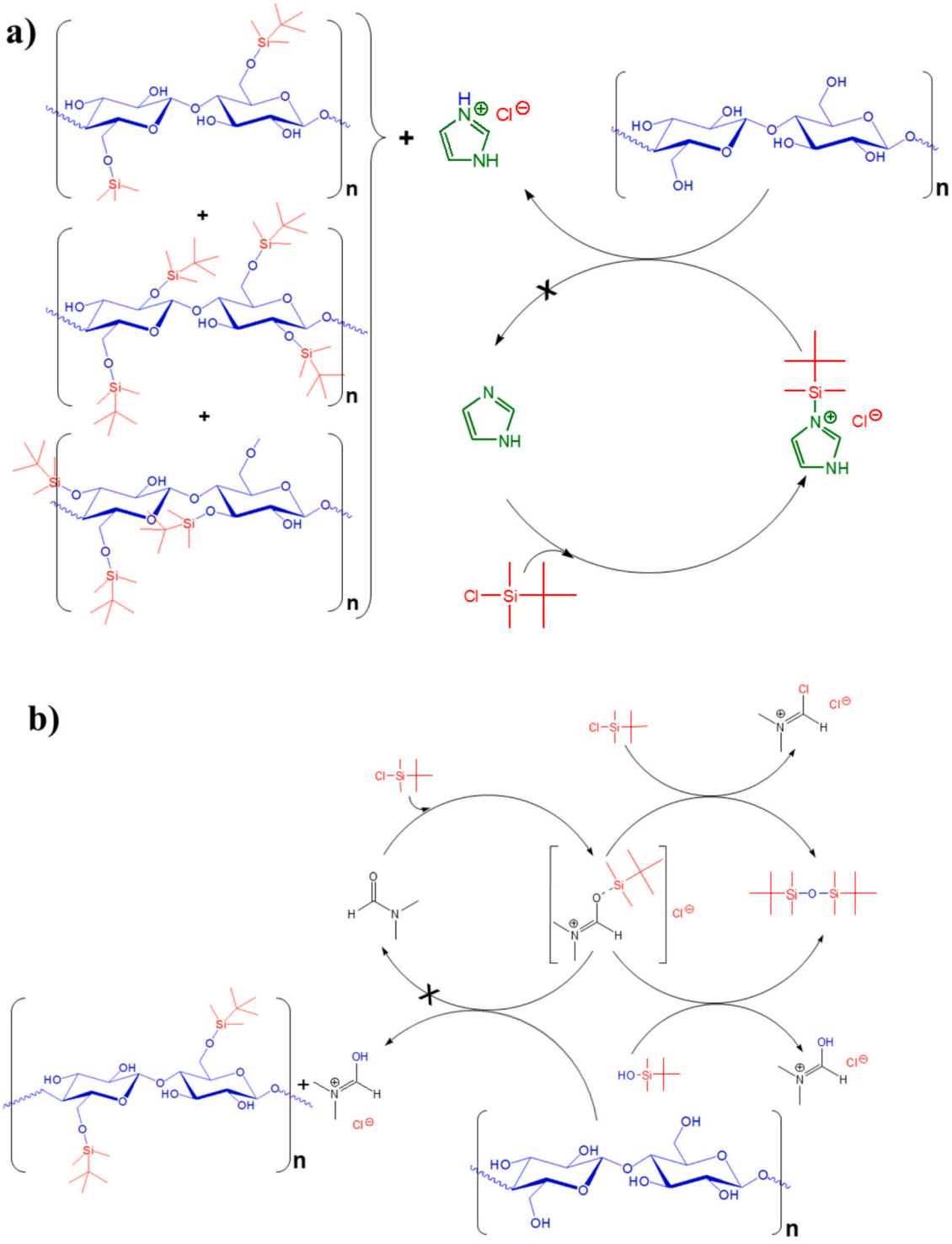

Fig. 1. Mechanism of KWP silylation in presence of: (a) TBDMSCl-imidazole and (b) TBDMSCl-DMF.

which is assigned to $(C—H)_{silyl}$ in-plane bending of the methyl group, a band at 838 cm^{-1} related to $Si-OH_{silyl}$ stretching vibration, and a band at 778 cm^{-1} related to $Si-C_{silyl}$ and $Si-O_{silyl}$ stretching vibration (Z. Zhang et al., 2014; Z. Zhang et al., 2015). The intensity of these bands increased with the reaction time, indicating the progress of the silylation process. Another change that confirmed the modification of KWP was the decrease in the band centred at ~3420 cm^{-1}, which is associated with the hydroxyl groups. This band decreased as the reaction time increased. Moreover, a distinct peak at approximately 1590 cm^{-1} was observed in the FTIR spectra of the silylated pulp samples. This band, which is masked in the spectrum of neat cellulose by a broad absorption around 1646 cm^{-1} due to the bending vibrations of water molecules physically adsorbed within the cellulose structure, became clearly distinguishable after surface modification. The appearance of the 1590 cm^{-1} band is commonly associated with the aromatic backbone vibrations of lignin and the asymmetric stretching of carboxylate (COO-) groups in hemicellulose (Horikawa et al., 2019; Md Salim et al., 2021). Its appearance may indicate partial exposure or enhanced detection of these components as a result of chemical modification, possibly due to decreased moisture interference and alterations in the surface chemical

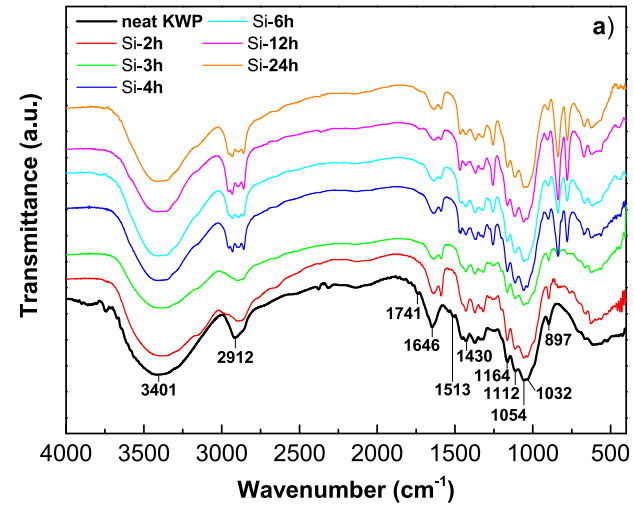

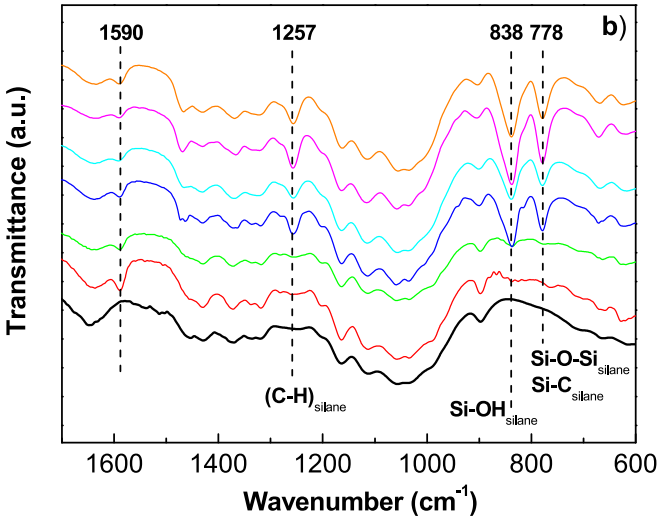

Fig. 2. FTIR spectra of KWP and silylated samples prepared at temperature of 40 °C and ratio of TBDMSCl/imidazole (1.5:2.5) as a function of reaction time.

environment induced by silylation.

The sum transmittance ratio for the new bands was normalized using the transmittance value at 1164 cm^{-1} of silylated samples as in previous work (Z. Zhang et al., 2014; Z. Zhang et al., 2015). This was estimated to determine the influence of the reaction time, temperature, and TBDMSCl/ImH ratio on the silylation process. The influence of these variables on the transmittance ratio is shown in Fig. 3. It is evident that an increase in the TBDMSCl/ImH ratio from 1/2.5 to 2.5/2.5 resulted in a linear increase in the A_{Si}/A_{CH} ratio (see Fig. 3a). This indicates that the amount of silylating agent available is a key factor in the efficiency of the reaction, since, together with the presence of imidazole as an auxiliary base and catalyst, it facilitates the activation of TBDMSCl, forming a highly efficient reactive intermediate for the transfer of the silyl group to the hydroxyls. This fact prevents premature decomposition of the silylating agent and favor a complete conversion, improving the reaction rate and avoiding unwanted side reactions (Corey & Venkateswarlu, 1972). Furthermore, in the silylation of glucopyranoses, the use of an insufficient amount of reagent resulted in incomplete protection, while an excess of TBDMSCl without a suitable base led to the formation of unwanted by-products and reduced stability of the polymer structure (Nouvel et al., 2003). On the other hand, raising the reaction temperature from 20 °C to 100 °C also resulted in an increase in the A_{Si}/A_{CH} ratio from 0.244 to 0.888, as shown in Fig. 3b. As can be also observed, the ratio increases slowly up to 40 °C but increases much faster after this temperature. This trend shows that elevated temperature improves the solubility and diffusion of reagents in the silylation process, favoring the efficiency of the reaction. The enhancement of silylation with the increasing temperature may be attributed to the fact that at higher temperatures, the reactants have greater mobility and the cellulosic fibers undergo greater expansion, facilitating access to the reactive hydroxyl groups (Chung et al., 2002). However, excessive temperature increases can have counterproductive effects, such as

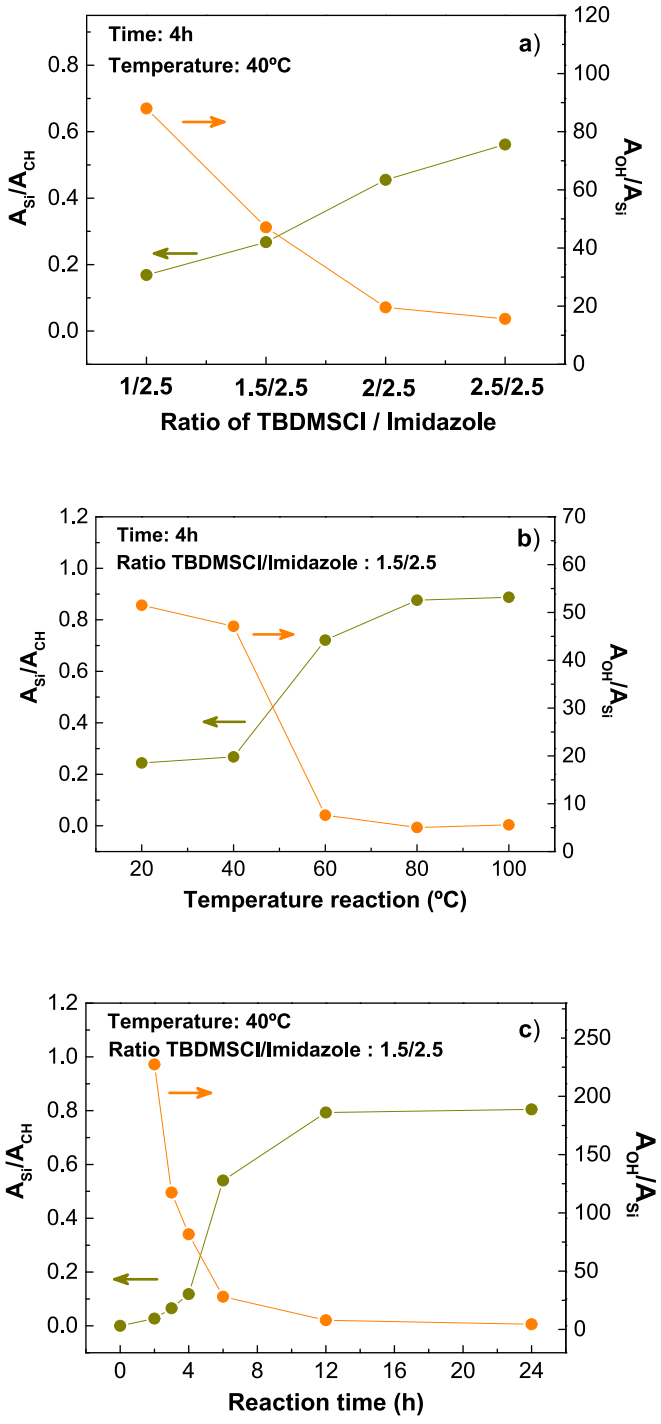

Fig. 3. Evolution of the transmittance ratio for the A_{Si}/A_{CH} and A_{OH}/A_{Si} with processing variables of silylation: (a) TBDMSCl/ImH ratio; (b) Reaction temperature; (c) Reaction time;

causing degradation of the polymer chains due to the thermal instability of the substrate (Nouvel et al., 2003) or promoting the formation of by-products that reduce the purity of the final product (Rojas-Escudero et al., 2004). This balance between factors favoring and hindering conversion could be the reason for the stabilization of the A_{Si}/A_{CH} slope at 80 °C. Reaction time was also found to play a fundamental role in the efficiency of silylation. Longer reaction times favor a more complete conversion of the hydroxyl groups of glucopyranoses (Arias-Pérez et al., 2002), which explains the significant increase in the A_{Si}/A_{CH} ratio, from 0.062 to 0.803, when increasing the reaction time from 4 h to 12 h (see Fig. 3c). This effect can be attributed to the positive impact of time on the intramolecular diffusion and adsorption of the reagents, which improves the contact between the TBDMSCl and the fibers (Bu & Rhee, 2000). After 12 h of reaction, the A_{Si}/A_{CH} ratio stabilized (see Fig. 3c), suggesting that the final silylation was achieved. This phenomenon could be explained by the steric hindrance created by the silane groups grafted onto the cellulose fibers, which prevents access to new reaction sites, or by the possible partial degradation of the silylating agent at high

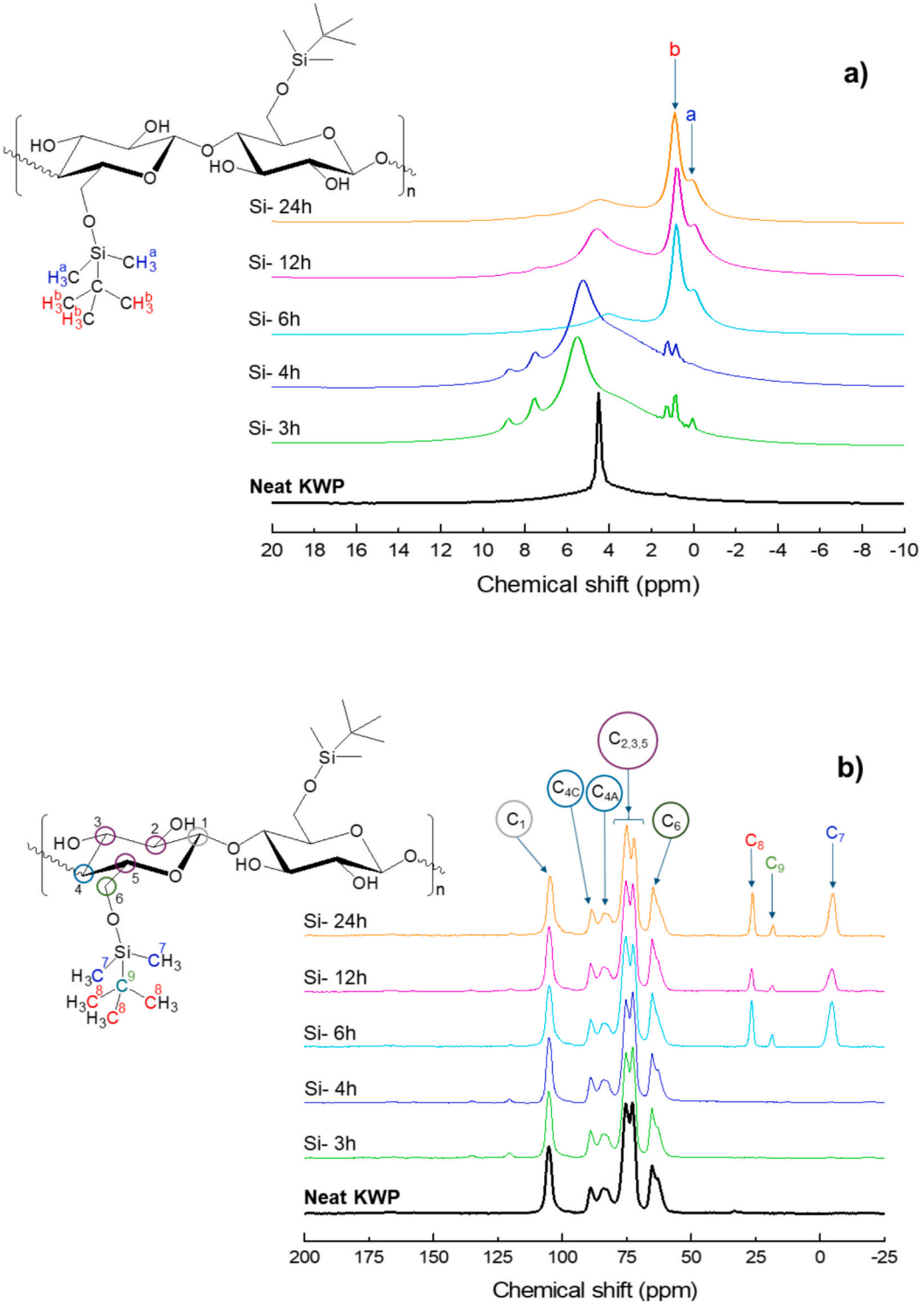

Fig. 4. (a) ^{1}H NMR; (b) ^{13}C NMR and (c) XPS survey - high-resolution spectra of neat KWP and silylated samples as a function of reaction time.

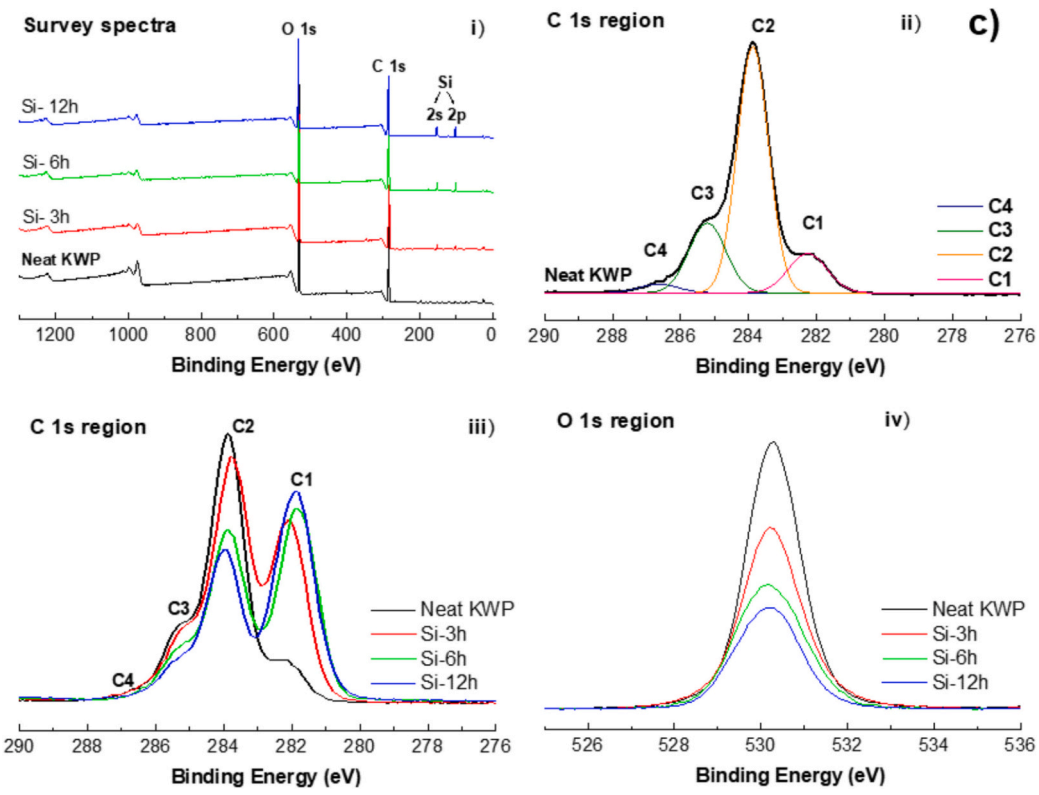

Fig. 4. (*continued*).

temperatures for long periods of time, which reduces the stability of the silyl group (Corey & Venkateswarlu, 1972). Therefore, as mentioned above, the modification of the fibers can lead to a significant reduction of the hydroxyl group and the appearance of the silane groups, which is a consequence of the appropriate reaction parameters. It is important to emphasize that the specific objective of this part of the study is not to optimize the above parameters, but rather to illustrate the flexibility of the proposed methodology to produce a wide range of suitable samples for modifying the rheological properties of bitumen and oil.

In order to characterize the chemical structure of the modified samples, ^{1}H NMR and ^{13}C NMR analyses were carried out. The spectra of the neat KWP and silylated samples as a function of reaction time are shown in Fig. 4. The ^{1}H NMR spectra show a peak at 3.5–5.5 ppm (see Fig. 4a) that includes all the protons of the glucopyranoside ring without being able to distinguish between them (Holding et al., 2016; Mittal et al., 2009). However, the ^{13}C NMR spectra give more information on the cellulose structure, with distinct peaks at 58–68 ppm due to the resonance of C_6, 68–80 ppm for C_2, C_3 and C_5 and 102–108 for C_1 (Baldoni et al., 2011; El Hariri Nokab et al., 2022). Two peaks were also observed at 80–85 ppm due to the (C_{4A}) of the amorphous cellulose fraction and 85–92 ppm of those C_4 of the crystalline fraction (C_{4C}) (Foston, 2014). New peaks were observed in the ^{1}H NMR spectra of the silylated samples due to the resonances of the protons of the introduced group (Fig. 4a). The resonance peak at 0.90–0.89 ppm was attributed to the protons of the Si-bounded tert-butyl group, while the peak at 0.11–0.06 ppm was associated with the methyl group of the silane (Benediktsdóttir et al., 2011; Buono et al., 2016; Glisin et al., 2024; Weldu & Wang, 2021). The integral of these peaks increases with increasing reaction time and therefore with increasing substituent concentration in the sample. It is noteworthy that a significant increase in substitution occurs after 4 h, since at shorter times these peaks are weaker and no significant changes are observed. The ^{13}C spectra support the ^{1}H results obtained on the Si-bonded carbons, showing clearly differentiated peaks at −4.7 ppm for the methyls, 18.8 ppm for the C—Si of the tert-butyl and 26.3 ppm for the methyls of the tert-butyl (Baldoni et al., 2011; Glisin et al., 2024). Again, these peaks are significant after 4 h, showing that the chemical modification occurs significantly after this time. The peaks at 7.50 and 8.70 ppm are due to the imidazole ring (Benhabbour et al., 2005), probably due to a deficiency in the purification process of the silylated samples. While the absence of a peak around −65 ppm (data not shown) displays that there are no reaction by-products such as *tert*-butyldimethylsiloxane (Z. Zhang et al., 2014).

X-ray photoelectron spectroscopy (XPS) analysis was also conducted to investigate the chemical changes resulting from the surface modification of cellulose pulp fibers. Fig. 4c-i presents the XPS survey spectra, showing electron intensity as a function of binding energy for both neat KWP and silylated samples. The neat KWP exhibits two primary peaks at approximately 531.3 eV and 284.8 eV, corresponding to oxygen (O 1 s) and carbon (C 1 s) atoms, respectively (García-Astrain et al., 2016; Tingaut et al., 2011). In addition to these main peaks, minor peaks associated with nitrogen (~399.8 eV for N 1 s), chlorine (~196.3 eV for Cl 2p), and calcium (~346.3 eV for Ca 2p) were also observed, indicating the presence of impurities in the wheat straw pulp. In contrast, the silylated samples exhibit two additional peaks at approximately 149.7 eV and 98.5 eV, attributed to Si 2 s and Si 2p, respectively. These peaks confirm the successful incorporation of silane groups onto the fiber surface (Khanjanzadeh et al., 2018; Souguir et al., 2012). Fig. 4c-ii shows the high-resolution scan of the C 1 s region for neat KWP. As observed, the spectrum can be deconvoluted into four distinct peaks (C1–C4), in agreement with previous studies (Andresen et al., 2006; Dhali et al., 2022; Montplaisir et al., 2008). The first peak (C1), at 282.3 eV, corresponds to C–C/C–H bonds. The second and most intense peak (C2), at 283.9 eV, represents C—O bonds. The third peak (C3), located at 285.2 eV, is attributed to acetal linkages (O–C–O), while the fourth peak (C4), at 286.6 eV, is associated with O–C=O groups. Fig. 4c-iii compares the high-resolution C 1 s spectra of neat KWP and silylated samples. Notably, as the reaction time increases, the intensity of the C1 peak progressively rises, while the C2 peak decreases. The increase in C1

intensity is indicative of C–C/C–Si bonding, reflecting a higher surface concentration of carbon and silicon due to silane group incorporation. This trend suggests a direct correlation between signal change and the degree of chemical modification. A similar decrease is observed in the C2 (C—O) peak and the 532.2 eV signal in the high-resolution O 1 s region (Fig. 4c-iv), which corresponds to C–OH bonds. This attenuation is attributed to the substitution of hydroxyl groups (Dhali et al., 2022; Jankauskait et al., 2020). In terms of elemental composition, neat KWP shows oxygen and carbon contents of 39.34 at.% and 58.48 at.%, respectively, yielding an O/C ratio of 0.67. This is consistent with values reported by (Sain & Panthapulakkal, 2006) for wheat straw fibers obtained via mechanical pulping. In contrast, the O/C ratios of silylated samples are lower, ranging from 0.56 to 0.33, indicating an increase in carbon content at the surface due to silane substitution. Silicon concentrations were measured at 1.18 at.%, 3.97 at.%, and 5.93 at.% for reaction times of 3, 6, and 12 h, respectively. These results confirm the successful chemical surface modification of the silylated samples.

The determination of degree of substitution (DS) was carried out through FTIR (M. Zhang & James, 2005) as a measure to quantify the chemical modification degree of the samples. These results were compared with ^{1}H NMR and ICP-OES measurements. As mentioned above, the silylation process involves the replacement of –OH by silane groups and this fact can be used to the determinate the DS (see Fig. 3a). The peak area assigned to –OH stretch vibration (A_{OH}) was measured and normalized with respect to the vibration band of cellulose skeleton overlap at 900–1200 cm^{-1} (Buono et al., 2016; Jankauskait et al., 2020). These peaks do not change during silylation and can be used as the reference (A_{ref}) to calculate the DS. Thus, the substitution degree was calculated as follows:

$$DS = 3 \times \left[\frac{\left(A_{OH}/A_{ref}\right)_{\text{neat KWP}} - \left(A_{OH}/A_{ref}\right)_{\text{silylated pulp}}}{\left(A_{OH}/A_{ref}\right)_{\text{neat KWP}}} \right] \quad (2)$$

In this equation, 3 represents the number of hydroxyl groups available on the D-glucose rings. Based on this expression, the Fig. 5a displays the evolution of DS as a function of silylation reaction time. The DS values increase with the reaction time up 1.5 for a reaction time of 12 h. These results confirm the theoretical prediction of the reaction mechanism (see Fig. 1), that the primary hydroxyl group in cellulose is much more reactive than the other two secondary hydroxyl groups and that only partial substitution of these groups finally occurs. Furthermore, since the *tert*-butyldimethylsilyl group is relatively bulky, the silylated samples at 12 and 24 h reaction times showed approximately the same DS, which can be considered the maximum value that can be obtained for these samples due to the steric effects caused by the *tert*-butyldimethylsilyl group. Figs. 5b-c display the evolution of the sum integral ratio of the protons due to the silicon with the protons of the glucopyranoside ring calculated by NMR (I_{Si}/I_{AGU}) and the percentage of silicon calculated by ICP-OES (% Si). Interestingly, all the curves exhibit the same trends with the silylation reaction time, corroborating the DS results.

X-ray diffraction analysis was used to estimate the influence of the silylation process on the crystallinity of samples. In the pulp, the cellulose has a crystalline structure due to hydrogen bonding interactions and van der Waals forces between the adjacent molecules, unlike hemicellulose and lignin, which were essentially amorphous (Chirayil et al., 2014). Fig. 6a shows the X-ray diffraction patterns of neat KWP and silylated samples as a function of reaction time. Neat KWP exhibited a dominant peak at approximately $2\theta = 22.3°$. Additionally, an average overlapped broad peak and a weak peak were observed at $2\theta = 15.7°$ and 34.5° respectively, which have been identified as corresponding to the (200) plane, the overlapped (1−10)/(110) planes and the (004) plane. This diffraction curve is the typical of cellulose I structure (French, 2014; French & Santiago Cintrón, 2013). The silylated samples showed a similar type of polymorphism. The crystallinity index of the neat KWP was 59.9 % determined using the Segal method. This value is

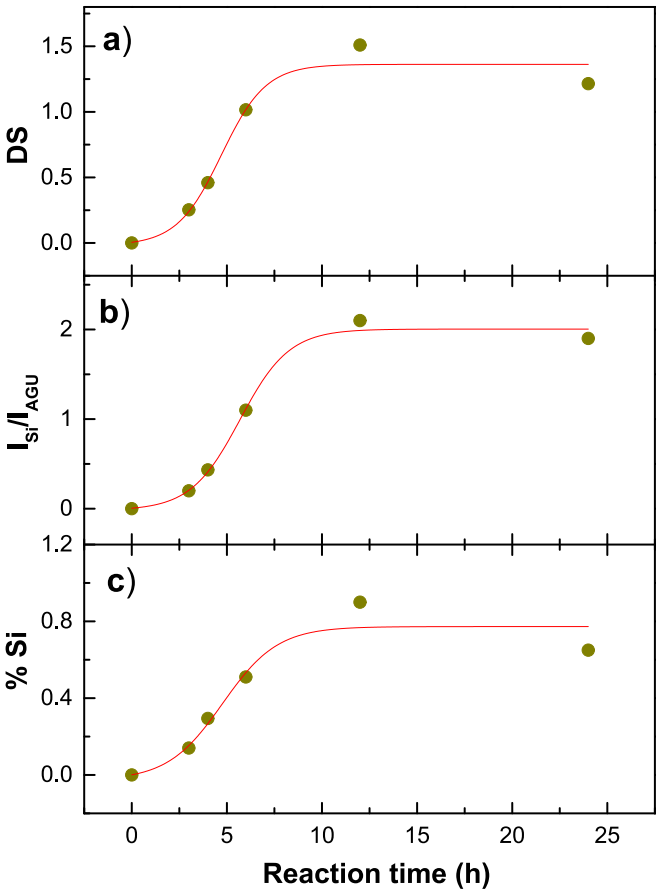

Fig. 5. Evolution of: (a) The degree of substitution (DS); (b) Sum integral ratio of the protons due to the silicon with the protons of the glucopyranoside ring calculated by NMR (I_{Si}/I_{AGU}); (c) The percentage of silicon calculated by ICP-OES (% Si) as a function of reaction time.

consistent with a previous study using similar wheat straw pulp (Espinosa et al., 2017). However, the patterns of the silylated samples from 6 h showed a clear decrease in the main peak at 22.3° with increasing reaction time, indicating a reduction in crystallinity, while samples silylated up to 4 h exhibited increased crystallinity (see Fig. 6b). These results may be explained by a double effect on the pulp during the silylation process. On one hand, the initial increase in the crystallinity index could be associated with a reduction of the amorphous portion of pulp fibers (i.e. content of extractives, and particularly lignin, see Table 1) due to the silylation process (Y. Chen et al., 2017; Tao et al., 2019). While the decrease in the crystallinity could be attributed to the chemical modification of pulp fibers due to the incorporation of the alkylsilane groups in the cellulose fibers.

In addition, contact angles were measured 1 and 60 s after the drop was applied to the sample surface in order to point out the silylation process effect on the hydrophobic behavior of the pulp fibers (see Fig. 6c). As expected, the obtained contact angle values were much higher than those found for the neat KWP. The unmodified pulp quickly absorbs the drop and the contact angle was reduced to 0. This highly hydrophilic character of lignocellulosic material is due to the abundance of hydroxyl groups on the surface of unmodified fibers. This corroborated the XPS results. Furthermore, the water contact angle increased as the silylation reaction time (i.e. degree of substitution) increased due to the substitution of surface hydroxyl groups by a higher content of silane groups and a corresponding decrease in polarity of the pulp fibers. Thus, the highest contact angle values were obtained for samples silylated at long reaction times (12 and 24 h), 46.57 and 66.94 respectively, while in both cases, the results illustrated no decrement in water droplet angle

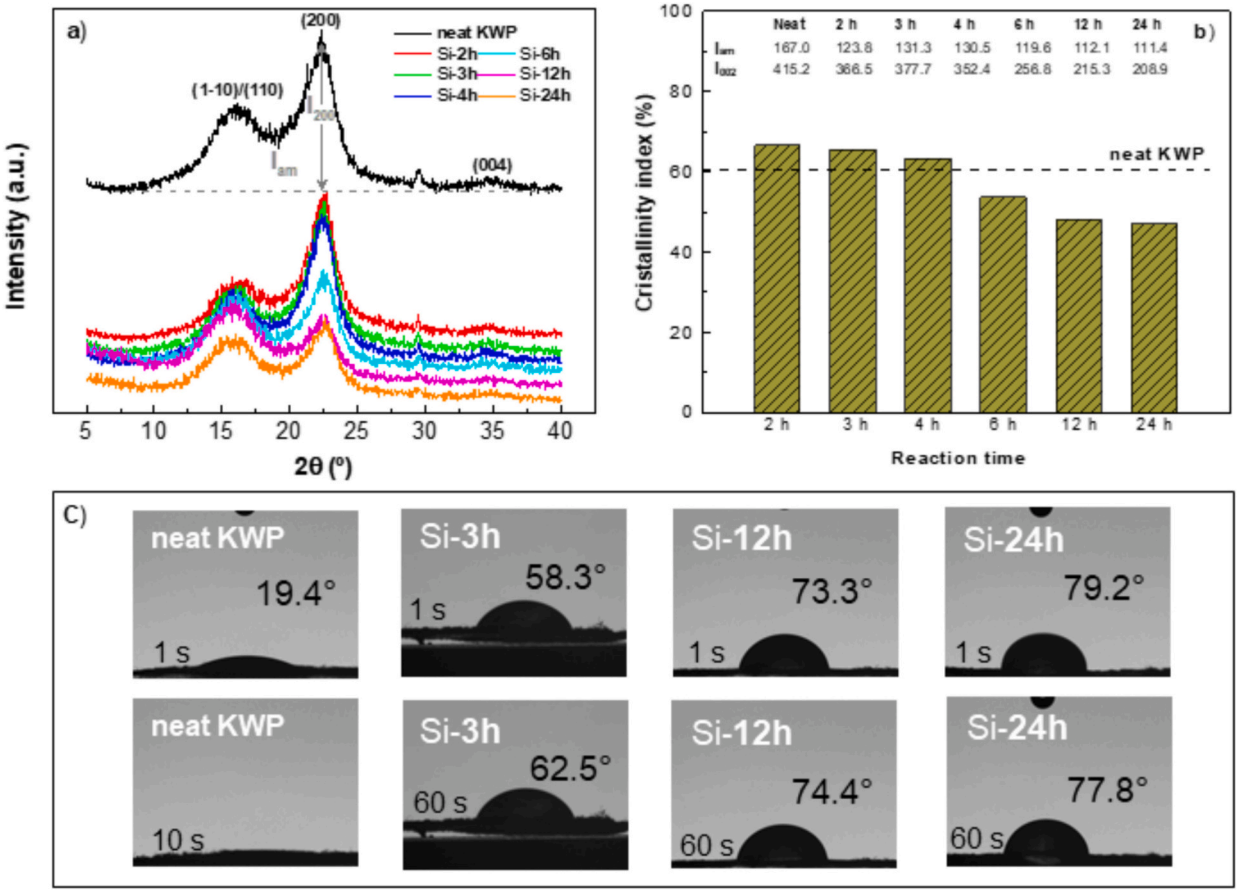

Fig. 6. (a) XRD diffractograms; (b) Crystallinity index; (c) Water contact angles of neat KWP and silylated samples as a function of reaction time.

even after 300 s observation. These results show that silylation changed the surface properties of the pulp fibers from highly hydrophilic to more hydrophobic and are in agreement with previous results, as it is known that the modification of cellulose with silanes and their derivatives increases the hydrophobicity of cellulosic substrates (Jing et al., 2022; Sayadi & Brouillette, 2024).

An examination of the fiber morphology before and after silylation was also carried out to assess the physical changes in the fibers. Fig. 7 displays selected micrographs of neat KWP and silylated samples obtained through SEM at magnifications of x100 and x1000, respectively. As can be observed, neat pulp appeared to be a compact and irregular fiber-like material with a smooth surface and a diameter of 5 ± 3.7 μm. This compact structure is the result of the intermolecular hydrogen bonding and the strong interactions between the cellulose chains (Jankauskaitė et al., 2020). Fiber morphology of the silylated samples retained its original shape, but the structure became less compact, and the diameter increased slightly (see the bar graphs of the fiber diameter distribution in the insets of Fig. 7). Similar results have been found by other authors for nanocrystalline cellulose chemically modified with methyltrimethoxysilane (Kim et al., 2018).

Thermogravimetric analysis (TGA) of neat KWP and silylated samples as a function of reaction time was evaluated to investigate their thermal behavior (see Fig. 8). Neat KWP showed a mass loss about 5.6 wt % below 100 °C, which can be attributed to the evaporation of water from cellulosic pulp (Espinosa et al., 2017). This mass loss decreases with the degree of modification of the pulp, confirming the higher hydrophobic character of the silylated samples. The thermal decomposition of neat KWP takes place in one single stage in the range of 250–400 °C. This stage involves the breakage of the bonds between cellulose, hemicellulose and lignin, thus reducing the degree of polymerization and leading to the formation of CO_2, H_2O and other hydrocarbon derivatives (Ramírez et al., 2014). However, silylated samples present two thermal decomposition steps, which can be easily distinguished by peaks in the derivative mass curve (see Fig. 8b). The increase or decrease of loss mass associated with these peaks was influenced by the reaction time. Shorter reaction times (2–4 h), achieved a clear increase of loss mass in the first stage. These results could be attributed to the fact that the alkylsilane produced was not strongly bound to the surface of fibers. Hence, this mass loss could be due to the elimination of low molecular weight species adsorbed on the surface of the cellulose fibers. On the other hand, for higher reaction times (> 4 h), there was no mass loss associated with the removal of alkylsilane groups (150–300 °C), confirming the strong adhesion of these groups. Zhang et al. reported similar thermal results of the silylated nanofibrillated cellulose associated with the formation of low molecular weight species adsorbed on the fibers surface (Z. Zhang et al., 2015). In addition, a decrease in the percentage of residue was observed with increasing reaction time (i.e. with the degree of substitution). Similar results were found by Mormann and Wagner et al. for silylated cellulose with hexamethyldisilazane (Mormann & Wagner, 2000).

3.2. *Influence of silylation process on rheological properties of oleo-dispersions*

The viscoelastic behavior of oleo-dispersions was determined by applying a constant shear stress amplitude within the linear viscoelastic range (LVR). Figs. 9a displays the mechanical spectra for oleo-dispersions formulated with a 10 wt% of cellulose pulp, as a function of reaction time. In all cases the storage modulus, G′, was higher than the loss modulus, G″, over the whole frequency range studied frequency, which is a common behavior of gel-like dispersions (D. Liu et al., 2011; J. E. Martín-Alfonso et al., 2018). However, different patterns were

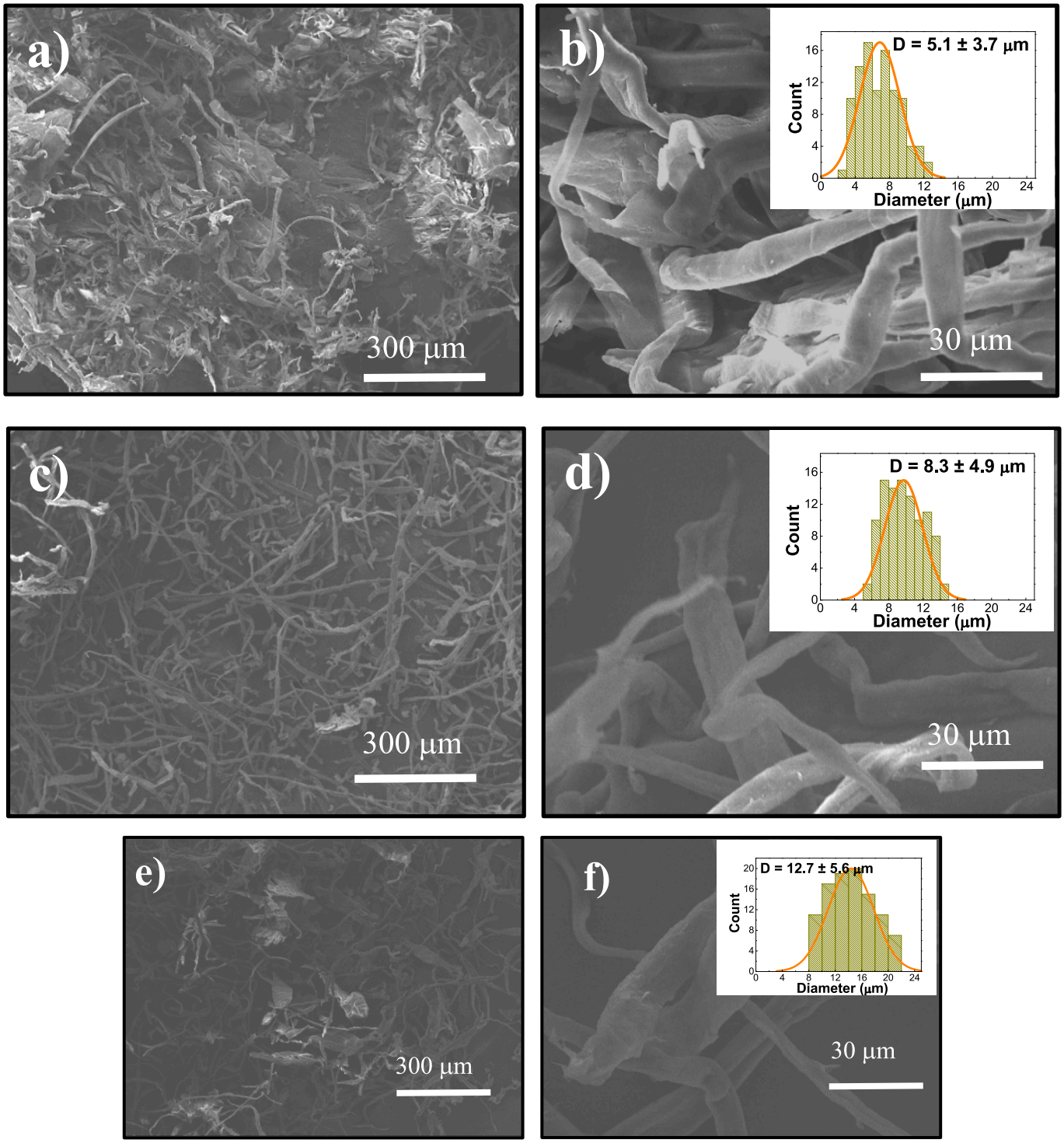

Fig. 7. SEM micrographs of selected samples: (a, b) neat KWP (x100 and x1000), (c, d) silylated 2 h (x100 and x1000) and (e, f) silylated 24 h (x100 and x1000).

found as a function of the reaction time. For oleo-dispersions formulated with neat KWP and silylated samples at low-intermediate reaction times (2–4 h), the mechanical spectra of the oleo-dispersions correspond to the so-called plateau relaxation zone, where G′ exhibited a weak frequency dependence, while G″ displayed a minimum. Nevertheless, silylated pulps processed at longer reaction times (6–24 h) produce gel-like dispersions with a poorly developed plateau region. Instead, both moduli increase almost in parallel. A value of 0.148 was obtained for the slope of the log-log plot of the elastic modulus versus frequency for these oleo-dispersions. This low value of the power law exponent relating G′ to frequency is characteristic of strong gels. These dispersions therefore meet the well-known Ross-Murphy criteria (Ross-Murphy, 1995) for strong gels. They cannot easily flow without undergoing shear induced fracture (see Fig. 9b), and the differences between G′ and G″ are sufficient to support the occurrence of a self-supporting gel. The different patterns found for the oleo-dispersions as a function of the reaction time could be directly related to the chemical modification of the pulp attributed to the silylation process. The group of samples silylated at lower reaction times showed a mechanical spectra similar to those of neat KWP, and the increase in viscoelastic moduli could be associated to

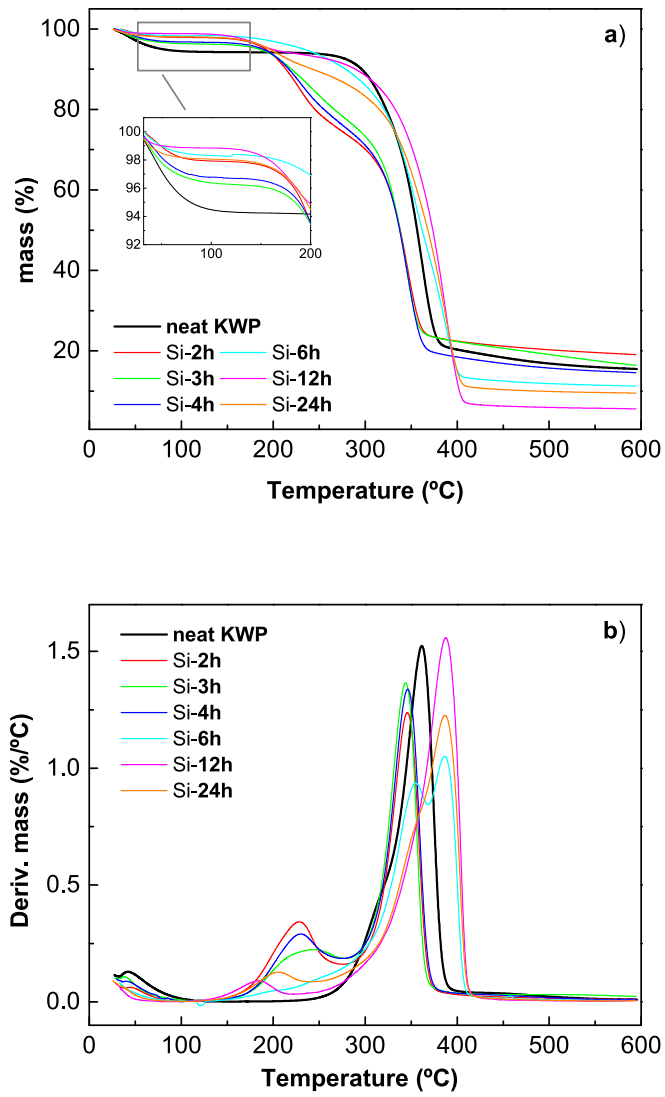

Fig. 8. Thermal behavior of neat KWP and silylated samples as a function of reaction time: (a) Thermogravimetric curves; (b) Deriv. mass curves.

the increase in crystallinity index (see Fig. 6b). In this sense, as it has been previously reported for lithium lubricating greases modified with polyolefins, the crystallinity degree was found the most highly influencing parameter on the rheological properties, increasing the viscoelastic moduli with the increase of this parameter (J. E. Martín-Alfonso et al., 2011; J. E. Martín-Alfonso, Valencia, et al., 2009). While the behavior of the pulp silylated with longer reaction times could be attributed to the higher compatibility of the fibers' pulp due to the higher chemical modification. It is worth noting that similar viscoelastic behavior with reaction times was found for oleo-dispersions formulated with acetylated cellulose pulp (Trejo-Cáceres et al., 2024).

Fig. 9d-f shows the physical appearance of selected samples once dispersed KWP in the oil medium, i.e. oleo-dispersions formulated with neat KWP and samples processed during the 4 h and 24 h. As can be observed, the oleo-dispersion formulated with neat KWP presents clear signal of partial phase separation, after 1 day from its preparation. However, a cohesive gel-like appearance was obtained for the silylated samples, with no signal of partial phase separation after 12 months of ageing. However, the oleo-dispersion prepared at low reaction time (3 h) showed a softer appearance with signs of the lubricant oil near the periphery of the fibers. While the oleo-dispersion formulated with pulp fiber with a higher DS display a more consistent and "drier" appearance. This supports the idea that silylation of the pulp significantly prevents the partial phase separation, i.e. the "oil bleeding" of the oleo-dispersions. Indeed, previous studies have shown that the modification of cellulose fibers with silanes and their derivatives significantly improves the hydrophobicity of cellulosic substrates (Jing et al., 2022; Sayadi & Brouillette, 2024). These results, associated with the physical stability of the samples, can also be confirmed by monitoring the mechanical spectra of the oleo dispersions over time, where the viscoelastic moduli showed similar values after 12 months of ageing, as shown in Fig. 9c. Furthermore, these selected oleo-dispersions were analyzed by SEM and the micrographs are illustrated in Fig. 9g-h. As can be seen, both oleo-dispersions display homogeneous and uniform microstructures similar to those found for the original pulp fibers (see Fig. 7c-f). No damage in the porous structure is apparent in the dispersions after mixing with castor oil, while the pore size seems to be reduced. In summary, the rheological properties of the oleo-dispersions are a consequence of the properties of the amphipathic fibers composed of hydrophilic and hydrophobic functional groups. The surface-modified wheat straw Kraft cellulose pulp, which contains hydrophobic alkylsiloxane segments, acts as a "bridge" to improve the compatibility between KWP and castor oil, promoting the transition from a liquid to a gel-like phase. This structuring effect is due to the formation of a three-dimensional network by chain entanglement and interactions between the pulp and the oil, resulting in microstructural stabilization of the oleo-dispersions.

Figs. 10a shows the influence of the pulp concentration on the mechanical spectra for oleo-dispersions formulated with cellulose pulp silylated for 3 h. The choice of this reaction time to assess the influence of thickener concentration was based on two reasons. Firstly, as shown above, this dispersion is physically stable and secondly, as shown in the Fig. 10a, it displays a mechanical spectrum similar to that of a conventional lithium grease and that the prepared at a higher time (4 h). As expected, it was found that an increase in pulp concentration was reflected in higher values of both G' and G'', indicating a progressive increase in the number of transient junction zones due to packing effects, which reduced the mobility of pulp fibers at high concentration values. This influence can be seen most clearly in the Fig. 10b, where the values of the storage viscoelastic modulus of the oleo-dispersions obtained from the mechanical spectrum at 1 rad/s are illustrated. In addition, the storage modulus values for lubricating greases formulated with lithium soap are also shown for comparison, adapted from previous works (J. E. Martín-Alfonso, Moreno, et al., 2009; Martín-Alfonso et al., 2013). G' clearly increases with both cellulose pulp and lithium-soap concentration. However, as can be seen, cellulose fibers have higher oil structuring capacity than lithium-soap. The anti-friction and anti-wear properties of the oleo-dispersions were also evaluated in a steel-steel sliding contact. Fig. 10c displays the curve for friction coefficient versus sliding time for the oleo-dispersions as a function of pulp concentration and a commercial lithium grease. Specific normal load (20N) and rotational speed (20 rpm) conditions were selected to achieve the elastohydrodynamic lubrication (EHL) conditions, previously determined by performing ramps of rotational speed, i.e., the Stribeck curves (see Fig. S1 of the supplementary material). EHL conditions can overlap into the mixed and boundary lubrication regimes and is the typical regime for friction pairs with elastic contact under high pressure and/or temperature conditions, such as ball bearings and gears (Rahnejat, 2010). At the beginning of the test both the oleo-dispersions and the lithium grease showed high values of the coefficient of friction, however these values gradually decreased until a steady state was reached. The high friction values initially obtained can be attributed to the absence of a protective lubricating film between the steel-steel interfaces, since the formation of a tribofilm is time-dependent (Çavdar & Ludema, 1991). The subsequent evolution of the coefficient, finally reaching almost constant values, confirms the formation of a protective film (M. A. Martín-Alfonso et al., 2022). As can be observed in the Fig. 10c, coefficient of friction values increased with the increasing silylated pulp concentration, presumably due to the lower oil-bleeding ability and the increase in internal friction

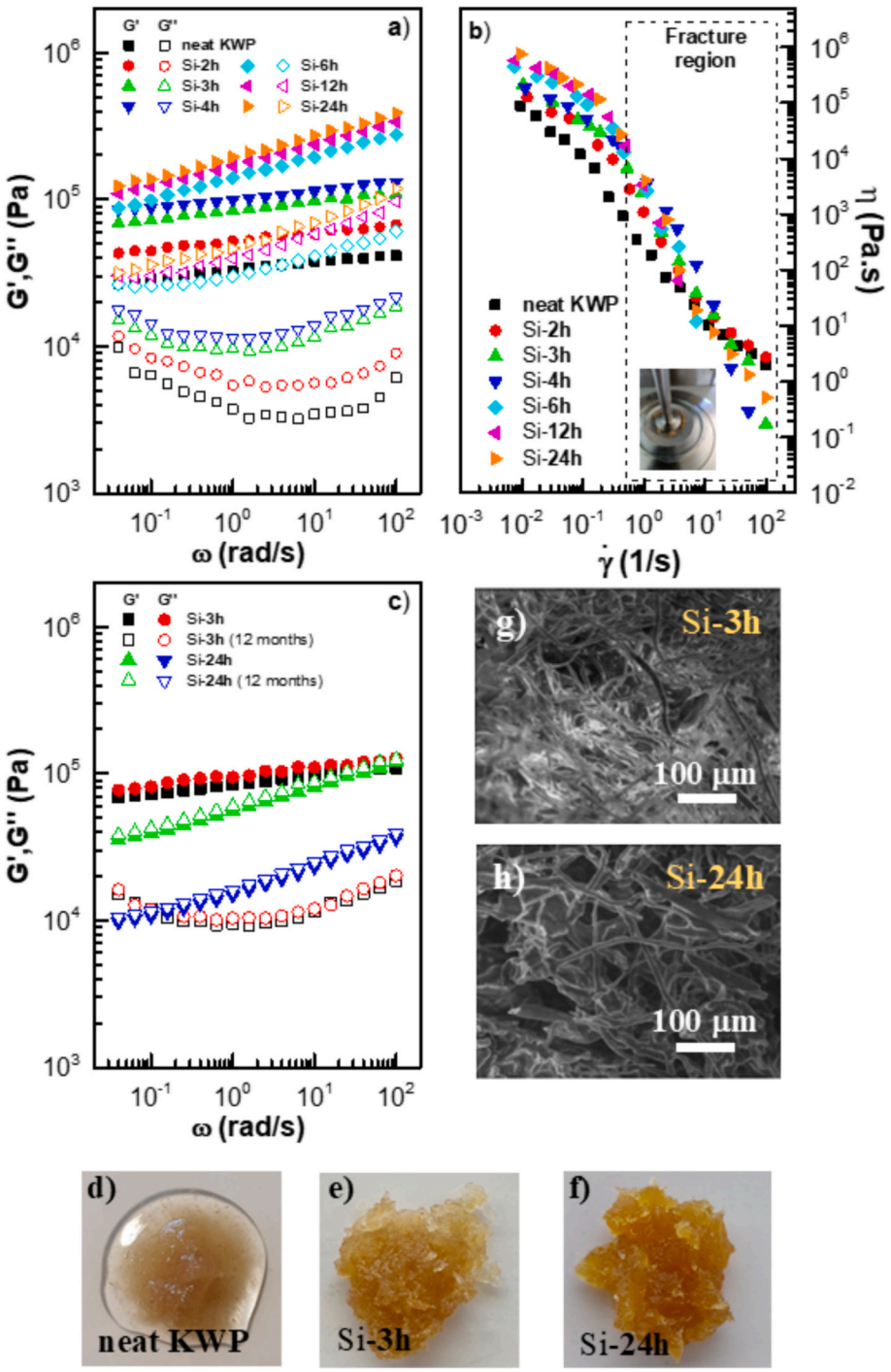

Fig. 9. (a) Viscoelastic properties of oleo-dispersions formulated with silylated samples as a function of reaction time. (b) Viscous flow curves of oleo-dispersions as a function of reaction time. (c) Viscoelastic properties of selected oleo-dispersions as a function of ageing time. Physical appearance of selected oleo-dispersions prepared with (d) neat KWP and silylated samples at (e) 3 h and (f) 24 h. SEM micrographs of selected oleo-dispersions prepared with silylated samples at (g) 3 h and (h) 24 h.

promoted by the thickener. A similar trend with thickener concentration was found for oleo-dispersions formulated with castor oil and eucalyptus kraft pulp or for oleogels formulated with ethylene–vinyl acetate copolymer and vegetable oils (J. E. Martín-Alfonso et al., 2018; J. E. Martín-Alfonso & Valencia, 2015). Interestingly, all oleo-dispersions showed lower friction factor values than the commercial lithium lubricating grease, being for the concentration with similar viscoelastic moduli (7.5 wt%) a 42 % lower. Fig. 10d-e shows the SEM images and corresponding wear surface profile of the worn surface on steel/steel contacts lubricated by selected oleo-dispersions and commercial lithium lubricating grease. As can be observed, the three worn surfaces present linear grooves in the sliding direction. Wear scar diameter and depth was reduced by decreasing the silylated pulp concentration until the wear was totally prevented below the 7.5 wt% (surface not shown), again revealing significant improvement with a lithium grease. According these results, it can be seen that a protective surface layer of silylated fibers and oil molecules is formed at the interface of the friction pair when lubricated by the oleo dispersions, thus preventing direct

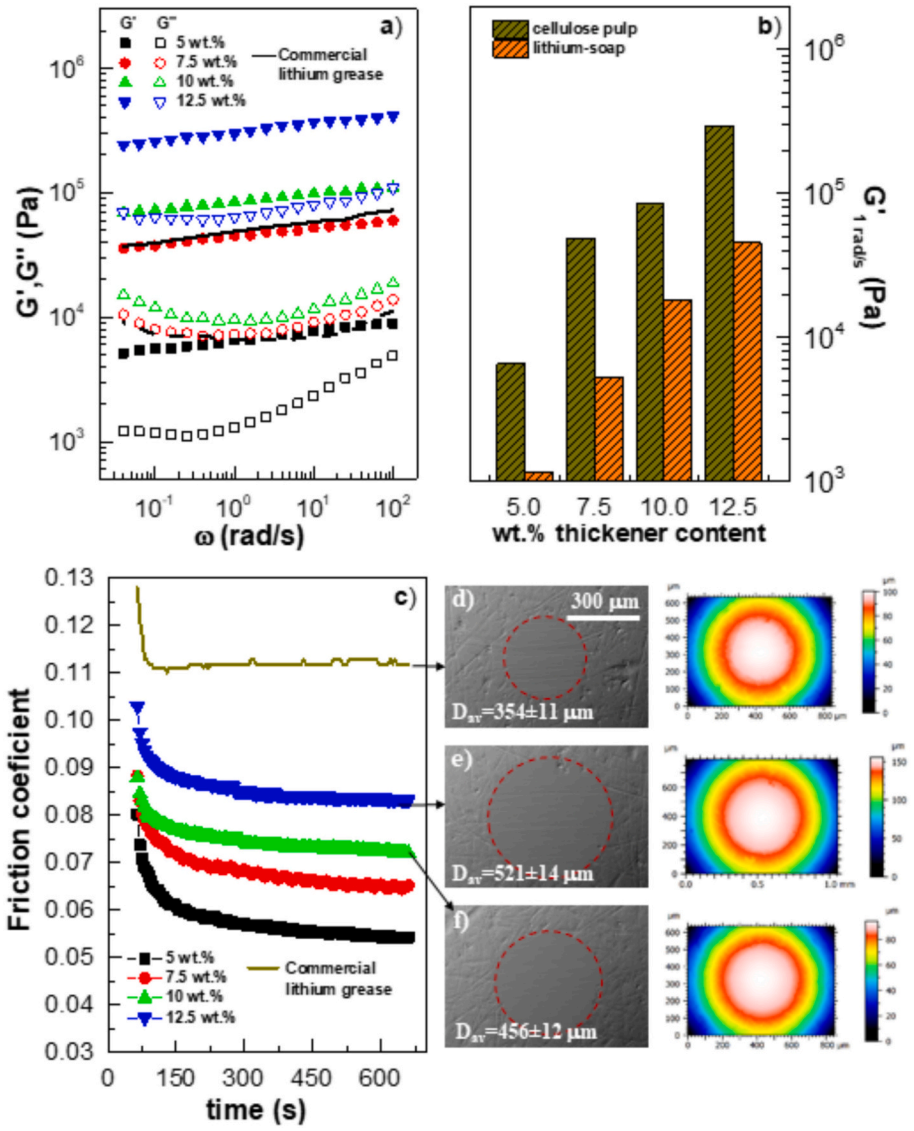

Fig. 10. (a) Viscoelastic properties of oleo-dispersions as a function of pulp concentration. (b) Evolution of storage modulus at 1 rad/s of oleo-dispersion and lithium grease as a function of thickener concentration. (c) Friction curves for oleo-dispersions as a function of pulp concentration. Wear mark appearances with their corresponding average diameter (D_{av}) and surface profile of (d) model lithium grease and (e, f) selected oleo-dispersion.

contact between the ball and the steel plate, thereby minimizing the friction and wear. The tribofilm formation is the result of a tribochemical reaction, polishing or rolling effects or a mixture of these, proposed as lubrication mechanisms to explain the process of friction (Kong et al., 2017). In this case, due to rod-like geometry of the cellulose fibers, a proper explanation is that the fibers fill in the grooves and scars of the friction surface and compensate for the loss of mass, which is known as the self-mending effect. This mechanism is supported by the fact that the surfaces lubricated by oleo-dispersions formulated with silylated samples were smoother than in the case of castor oil (Cortés-Triviño et al., 2019) and lithium grease (see the surface profiles in the Fig. 10d-f), even to the point that the wear was totally prevented, and this level of surface roughness was reasonable for the compensation using this type of fiber (see Fig. 7). In addition, we believe that because the silane groups can be adsorbed on the steel interface, tribochemical reactions between Fe, Si and O may be initiated promoted by the frictional forces and generated heat. As a result, the chemical transfer film composed of iron oxides and silicon oxides can be formed, which has been reported to be highly resistant to friction and wear (B.-S. Zhang, Xu, Xu, et al., 2011; B. Zhang, Xu, Gao, et al., 2011).

3.3. *Influence of silylation on the rheological properties of bitumen-dispersions*

Fig. 11 displays the viscous flow curves, at 135 and 165 °C, for the bitumen and dispersions formulated with neat KWP and silylated samples. The knowledge of the viscosity values of the dispersions at these temperatures are of particular interest as these are typical handling, laydown and compaction temperatures (Cuadri et al., 2014). As can be seen, neat bitumen exhibits Newtonian behavior, i.e. the viscosity values are constant as the shear rate increases. On the contrary, bitumen dispersions show a shear thinning behavior with fluctuations, especially for sample formulated with neat KWP at low shear rates. Moreover, higher degrees of substitution, i.e. higher reaction times applied, causes a slight increase in shear viscosity of the dispersion. A similar pattern was observed at the temperature of 165 °C (see Fig. 11b). These results could be attributed to the pulp fiber shape and the structural network created in the dispersion, where the physical interaction between fibers, orientation and breakdown of flocs play a key role as evidenced by the behavior and viscosity fluctuations in the viscous flow curves. By increasing the shear rate, fiber structural networks and fiber flocs are

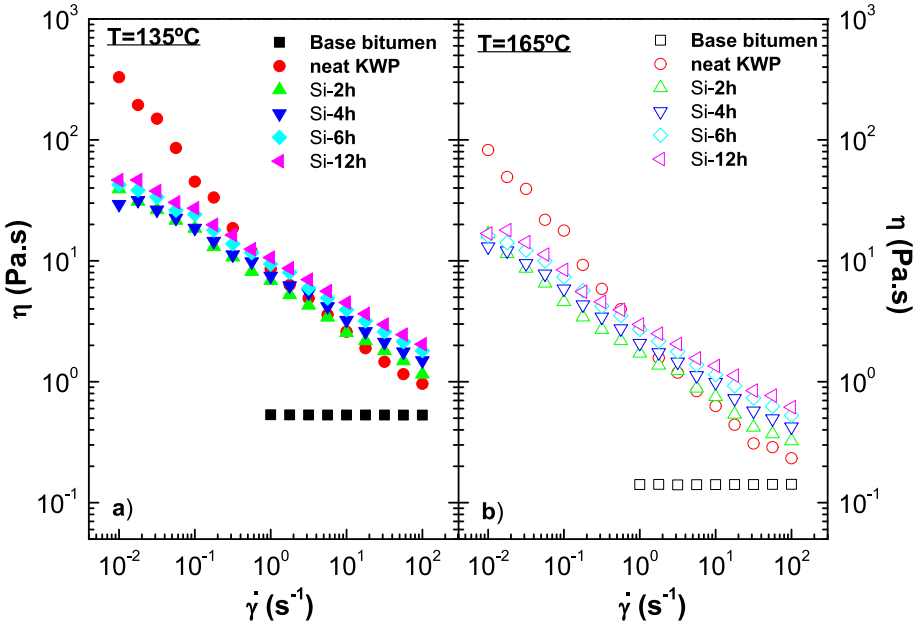

Fig. 11. Viscous flow curves, at 135 and 165 °C for the bitumen and dispersions formulated with neat KWP and silylated samples at different reaction times.

destroyed, leading to a decrease in viscosity and making the dispersion easier to flow, thus causing the shear-thinning behavior. Similar shear thinning pattern was described by (Derakhshandeh et al., 2010) for the commercial pulp fiber suspensions.

The linear viscoelastic behavior of the bitumen and dispersions formulated with neat KWP and silylated pulp was also studied by means of dynamic temperature sweep tests in the medium temperature interval. The complex shear modulus (G*) and phase angle (δ) were assessed, which mutually describe the viscoelastic response of dispersions. G*could be used to evaluate the rutting potential of the dispersion. A high G* indicates that it is a stiffer dispersion at the test temperatures, and that it has the potential to resist permanent deformation. However, the δ represents the time lag between the applied shear stress and the resulting shear strain. When $\delta = 0°$, the subject dispersion is a purely elastic material, and when $\delta = 90°$, it is a purely Newtonian viscous material. As can be seen in the Fig. 12a, for bitumen and dispersions formulated with neat KWP and silylated pulp with lower reaction times, the values of G* always decrease as temperature increases. However, the base bitumen presents lower stiffness (lower G* value) over the entire temperature interval tested in comparison to neat KWP and silylated pulp blends. The stiffening of the dispersions could be associated to the formation of a structural network due to the packing effect provided by the pulp fibers (Desseaux et al., 2018) within the bitumen matrix. Further, according to previous physicochemical characterization of the modified samples, the silylated fibers are composed of the silane group, which is constructive to the adhesion of bitumen (Cuadri et al., 2015). In

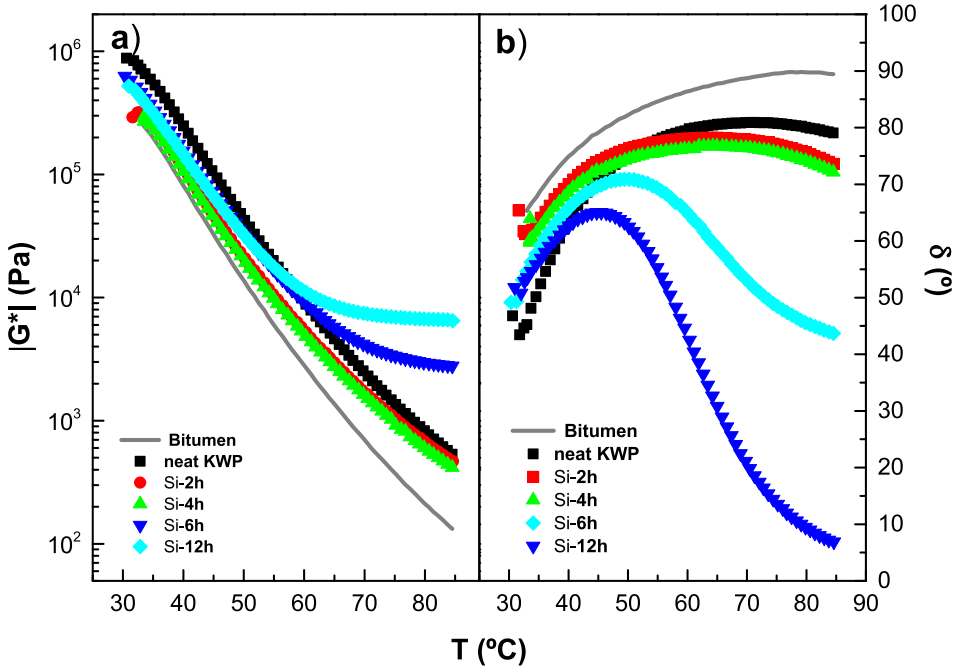

Fig. 12. Evolution with temperature of (a) complex shear modulus (|G*|) and (b) phase angle (δ) obtained for bitumen and dispersions formulated with neat KWP and silylated samples at different reaction times.

this sense, bitumen dispersions formulated with silylated pulp fiber obtained with higher reaction times (6 h and 12 h) do not exhibit a similar thermo-rheological behavior than bitumen or neat KWP at medium temperatures, reaching a G* plateau at about 65 °C. This shoulder in the viscoelastic moduli has been previously described for binders containing styrene–butadiene rubber (SBS) and polypropylene-glycol functionalized with polymeric 4,4-diphenylmethane diisocyanate (MDI-PPG) (Cuadri et al., 2014; Martínez-Boza et al., 2000), and shows that the addition of these modified fibers improves the temperature susceptibility of bitumen, in terms of hardness. Therefore, dispersions formulated with silylated pulp reacted for 6 or 12 h display higher G* values than base bitumen in this testing temperature range, which would indicate higher resistance to permanent deformation. The phase angle (δ) could be considered, in terms of viscoelastic behavior, more sensitive to the chemical structure and therefore the modification of bitumen than viscoelastic moduli (F. Chen, Taylor, et al., 2015). As can be seen in the Fig. 12b, the evolution of the phase angle with temperature for base bitumen displays a typical sigmoidal curve. Bitumen dispersions formulated with neat KWP and silylated pulp fiber with lower reaction times showed a similar behavior but with lower δ values for the silylated pulps. Hence, the results show that the dispersions containing silylated pulps have more elastic behavior than the bitumen and neat KWP blend. In addition, very interesting results were obtained for the bitumen dispersions formulated with samples modified with higher reaction times, since the phase angle shows a maximum between 45 and 55 °C, followed by a decrease of the values down to below 45°. This means that the samples undergo a transition from liquid-like to solid-like upon heating. In this respect, silylated pulp fibers with higher reaction times extend the temperature range of binder application. As previously mentioned above, these results could be associated with the excellent interaction between the alkyl-siloxane segments of the silylated fibers and the components of the bitumen which significantly increases the viscosity, accompanied by a transition from Newtonian (bitumen) to non-Newtonian behavior. Furthermore, the change in the complex shear modulus and phase angle of the bitumen-dispersions obtained also indicates the formation of a three-dimensional network due to chain entanglements and interactions between the silylated fiber and bitumen, which improves the rheological properties of the dispersions, similar to those found with SBS and MDI-PPG binders. In support of these findings, recent articles (Aldagari et al., 2022; Karnati et al., 2020; Shariati et al., 2023) have demonstrated that surface functionalization of nanoparticles with silane coupling agents significantly improves the dispersion of these nanoparticles due to excellent interaction in the bitumen matrix.

4. Conclusions

New hydrophobic materials based on wheat straw as lignocellulosic biomass from agricultural feedstock were successfully synthesized by silylation reaction and validated as sustainable rheological modifiers of two of the most industrially important hydrophobic fluids (bitumen and oil), with the aim of developing sustainable bitumen binders and semi-solid lubricant formulations. The silylation of wheat straw cellulose pulp (KWP) with *tert*-butyldimethylsilyl chloride (TBDMSCl) was proceeded in the presence of dimethylformamide and imidazole (ImH) as a catalyst, and different levels of silylation were obtained by adjusting the conditions of the reaction, such as reaction time (2–24 h), reaction temperature (20–100 °C) and TBDMSCl/ImH ratio (1/2.5–2.5/2.5), which illustrates the flexibility of the proposed methodology. The combined and comprehensive FTIR, NMR, and ICP-OES analyses conclusively demonstrate the effective silylation of KWP structure with substitution taking place preferably at C_6 positioned hydroxyl groups. The highest degrees of modification were obtained at 40 °C with a ratio of TBDMSCl/ImH: 1.5/2.5 after a reaction time of 12 h (DS ~ 1.6). XRD analysis revealed that the silylation process increased or decreased the crystallinity of the cellulose pulp depending on the reaction time. The SEM study showed that the silylated fibers retained their original shape and were slightly larger in diameter. Additionally, the thermal stability of the KWP was improved after 4 h of silylation, which was attributed to the inherent heat resistance of the silyl group adequacy bonded to the surface of the cellulose fibers. Silylated KWP samples were validated as rheological modifiers and structuring agents in oil and bitumen media. The chemical modification of KWP achieved during the silylation process has a significant impact on the linear viscoelastic functions of oil and bitumen dispersions, which was associated to the entanglement network formed due to the hydrophobic surface modification of the fibers with alkyl-silane group, confirming the initial hypothesis. Silylated KWP samples processed at intermediate reaction times (3–4 h) were able to form physically stable oleo-dispersions in castor oil, with adequate rheological and tribological properties, similar to those obtained with commercial lithium lubricating grease. While the filler effect provided by the pulp fibers and the stronger interactions developed specially between the silylated pulp fibers with higher degree of modification and the bitumen increase the stiffening and elasticity respect to the neat bitumen and the blend of this with non-modified KWP.

In the light of the results obtained, this approach dealing with the preparation of hydrophobic materials based on wheat straw, considered an abundant and non-expensive lignocellulosic biomass from agricultural feedstock, prove that tailoring the silylation degree is an effective and straightforward strategy to optimize and/or tune the rheological properties of hydrophobic fluids. Moreover, this innovative approach should open up new possibilities for the development of sustainable synthetic binders and semi-solid lubricants with novel functional properties, driving an initiative towards the valorization of these underutilized residues and the adoption of circular economy principles.

CRediT authorship contribution statement

M. Trejo-Cáceres: Writing – original draft, Validation, Methodology, Investigation, Formal analysis, Data curation, Conceptualization. **J. E. Martín-Alfonso:** Writing – review & editing, Writing – original draft, Validation, Supervision, Resources, Project administration, Methodology, Investigation, Funding acquisition, Formal analysis, Data curation, Conceptualization. **J.M. Franco:** Writing – review & editing, Validation, Supervision, Resources, Project administration, Methodology, Investigation, Funding acquisition, Formal analysis, Data curation, Conceptualization.

Declaration of competing interest

The authors of this paper declare that there is no conflict of interest.

Acknowledgments

This work was supported by GreenAsphalt project (grant number: 802C1800001), co-funded by FEDER European Programme (80 %) and Junta de Andalucía (Consejería de Economía, Conocimiento, Empresas y Unversidades/Agencia-IDEA). It has been also co-funded by FEDER European Programme and Junta de Andalucía (grant number: PY20_00751), and by MCIN/AEI/10.13039/501100011033 and "ERDF A way of making Europe" (grant number: PID2021–125637OB-I00). Funding for open access charge: Universidad de Huelva/CBUA.

Appendix A. Supplementary data

Supplementary data to this article can be found online at https://doi.org/10.1016/j.carbpol.2025.123778.

Data availability

Data will be made available on request.

References

Abdelwahab, M. A., Jacob, S., Misra, M., & Mohanty, A. K. (2021). Super-tough sustainable biobased composites from polylactide bioplastic and lignin for bio-elastomer application. *Polymer, 212*, Article 123153.

Adenekan, K., & Hutton-Prager, B. (2019). Sticky hydrophobic behavior of cellulose substrates impregnated with alkyl ketene dimer (AKD) via sub-and supercritical carbon dioxide. *Colloids and Surfaces A: Physicochemical and Engineering Aspects, 560*, 154–163.

Åkerholm, M., Hinterstoisser, B., & Salmén, L. (2004). Characterization of the crystalline structure of cellulose using static and dynamic FT-IR spectroscopy. *Carbohydrate Research, 339*(3), 569–578. https://doi.org/10.1016/j.carres.2003.11.012

Aldagari, S., Hung, A. M., Shariati, S., Faisal Kabir, S. K., Ranka, M., Bird, R. C., & Fini, E. H. (2022). Enhanced sustainability at the bitumen-aggregate interface using organosilane coating technology. *Construction and Building Materials, 359*, Article 129500. https://doi.org/10.1016/j.conbuildmat.2022.129500

Andresen, M., Johansson, L.-S., Tanem, B. S., & Stenius, P. (2006). Properties and characterization of hydrophobized microfibrillated cellulose. *Cellulose, 13*(6), 665–677. https://doi.org/10.1007/s10570-006-9072-1

Arancibia, F., Izquierdo, E., & Pereira, M. (2021). Stabilization of the emulsion of alkenyl succinic anhydride (ASA) in water using cellulose nanofibrils. *Chemical Engineering Science, 233*, Article 116407.

Arias-Pérez, M. S., López, M. S., & Santos, M. J. (2002). Imidazole-promoted 1,4-migration of the tert-butyldiphenylsilyl group: Influence on the selectivity control of the silylation reactions of carbohydrate OH groups. *Journal of the Chemical Society, Perkin Transactions 2, 9*, 1549–1552. https://doi.org/10.1039/B204396C

Baldoni, L., Stortz, C. A., & Marino, C. (2011). Synthesis and conformational analysis of 1,2-cis fused bicyclic α-d-galactofuranosyl thiocarbamate from per-O-tert-butyldimethylsilyl-β-d-galactofuranosyl isothiocyanate. *Carbohydrate Research, 346*(2), 191–196. https://doi.org/10.1016/j.carres.2010.11.013

Bangar, S. P., Kajla, P., & Ghosh, T. (2023). Valorization of wheat straw in food packaging: A source of cellulose. *International Journal of Biological Macromolecules, 227*, 762–776. https://doi.org/10.1016/j.ijbiomac.2022.12.199

Bendahou, A., Hajlane, A., Dufresne, A., Boufi, S., & Kaddami, H. (2015). Esterification and amidation for grafting long aliphatic chains on to cellulose nanocrystals: A comparative study. *Research on Chemical Intermediates, 41*, 4293–4310.

Benediktsdóttir, B. E., Gaware, V. S., Rúnarsson, Ö. V., Jónsdóttir, S., Jensen, K. J., & Másson, M. (2011). Synthesis of N,N,N-trimethyl chitosan homopolymer and highly substituted N-alkyl-N,N-dimethyl chitosan derivatives with the aid of di-tert-butyldimethylsilyl chitosan. *Carbohydrate Polymers, 86*(4), 1451–1460. https://doi.org/10.1016/j.carbpol.2011.06.007

Benhabbour, S. R., Chapman, R. P., Scharfenberger, G., Meyer, W. H., & Goward, G. R. (2005). Study of imidazole-based proton-conducting composite materials using solid-state NMR. *Chemistry of Materials, 17*(6), 1605–1612. https://doi.org/10.1021/cm0483011

Bu, J., & Rhee, H. K. (2000). Silylation of Ti MCM 41 by trimethylsilyl imidazole and its effect on the olefin epoxidation with aqueous H 2 O 2. *Catalysis Letters, 66*, 245–249.

Buono, P., Duval, A., Verge, P., Averous, L., & Habibi, Y. (2016). New insights on the chemical modification of lignin: Acetylation versus Silylation. *ACS Sustainable Chemistry & Engineering, 4*(10), 5212–5222. https://doi.org/10.1021/acssuschemeng.6b00903

Carrillo, F., Colom, X., Suñol, J., & Saurina, J. (2004). Structural FTIR analysis and thermal characterisation of lyocell and viscose-type fibres. *European Polymer Journal, 40*(9), 2229–2234. https://doi.org/10.1016/j.eurpolymj.2004.05.003

Çavdar, B., & Ludema, K. C. (1991). Dynamics of dual film formation in boundary lubrication of steels part III. Real time monitoring with ellipsometry. *Wear, 148*(2), 347–361. https://doi.org/10.1016/0043-1648(91)90294-5

Chen, F., Taylor, N., Kringos, N., & Birgisson, B. (2015). A study on dielectric response of bitumen in the low-frequency range. *Road Materials and Pavement Design, 16*(sup1), 153–169. https://doi.org/10.1080/14680629.2015.1029682

Chen, H., Ferrari, C., Angiuli, M., Yao, J., Raspi, C., & Bramanti, E. (2010). Qualitative and quantitative analysis of wood samples by Fourier transform infrared spectroscopy and multivariate analysis. *Carbohydrate Polymers, 82*(3), 772–778.

Chen, Y., He, Y., Fan, D., Han, Y., Li, G., & Wang, S. (2017). An efficient method for cellulose Nanofibrils length shearing via environmentally friendly mixed Cellulase pretreatment. *Journal of Nanomaterials, 2017*, 1–12. https://doi.org/10.1155/2017/1591504

Chen, Z., Hu, T. Q., Jang, H. F., & Grant, E. (2015). Modification of xylan in alkaline treated bleached hardwood Kraft pulps as classified by attenuated total-internal-reflection (ATR) FTIR spectroscopy. *Carbohydrate Polymers, 127*, 418–426. https://doi.org/10.1016/j.carbpol.2015.03.084

Chirayil, C. J., Joy, J., Mathew, L., Mozetic, M., Koetz, J., & Thomas, S. (2014). Isolation and characterization of cellulose nanofibrils from Helicteres isora plant. *Industrial Crops and Products, 59*, 27–34. https://doi.org/10.1016/j.indcrop.2014.04.020

Chung, M.-K., Orlova, G., Goddard, J. D., Schlaf, M., Harris, R., Beveridge, T. J., … Hallett, F. R. (2002). Regioselective Silylation of sugars through palladium nanoparticle-catalyzed Silane Alcoholysis. *Journal of the American Chemical Society, 124*(35), 10508–10518. https://doi.org/10.1021/ja026723v

Corey, E. J., & Kim, C. U. (1972). New and highly effective method for the oxidation of primary and secondary alcohols to carbonyl compounds. *Journal of the American Chemical Society, 94*(21), 7586–7587. https://doi.org/10.1021/ja00776a056

Corey, E. J., & Venkateswarlu, A. (1972). Protection of hydroxyl groups as tert-butyldimethylsilyl derivatives. *Journal of the American Chemical Society, 94*(17), 6190–6191.

Cortés-Triviño, E., Valencia, C., Delgado, M. A., & Franco, J. M. (2019). Thermo-rheological and tribological properties of novel bio-lubricating greases thickened with epoxidized lignocellulosic materials. *Journal of Industrial and Engineering Chemistry, 80*, 626–632. https://doi.org/10.1016/j.jiec.2019.08.052

Cuadri, A. A., Carrera, V., Izquierdo, M. A., García-Morales, M., & Navarro, F. J. (2014). Bitumen modifiers for reduced temperature asphalts: A comparative analysis between three polymeric and non-polymeric additives. *Construction and Building Materials, 51*, 82–88. https://doi.org/10.1016/j.conbuildmat.2013.11.009

Cuadri, A. A., Partal, P., Ahmad, N., Grenfell, J., & Airey, G. (2015). Chemically modified bitumens with enhanced rheology and adhesion properties to siliceous aggregates. *Construction and Building Materials, 93*, 766–774. https://doi.org/10.1016/j.conbuildmat.2015.05.098

Derakhshandeh, B., Hatzikiriakos, S. G., & Bennington, C. P. J. (2010). Rheology of pulp suspensions using ultrasonic Doppler velocimetry. *Rheologica Acta, 49*(11−12), 1127–1140. https://doi.org/10.1007/s00397-010-0485-2

Desseaux, S., dos Santos, S., Geiger, T., Tingaut, P., Zimmermann, T., Partl, M. N., & Poulikakos, L. D. (2018). Improved mechanical properties of bitumen modified with acetylated cellulose fibers. *Composites Part B: Engineering, 140*, 139–144. https://doi.org/10.1016/j.compositesb.2017.12.010

Dhali, K., Daver, F., Cass, P., & Adhikari, B. (2022). Surface modification of the cellulose nanocrystals through vinyl silane grafting. *International Journal of Biological Macromolecules, 200*, 397–408. https://doi.org/10.1016/j.ijbiomac.2022.01.079

Dimakos, V., & Taylor, M. S. (2018). Site-selective functionalization of hydroxyl groups in carbohydrate derivatives. *Chemical Reviews, 118*(23), 11457–11517. https://doi.org/10.1021/acs.chemrev.8b00442

El Hariri Nokab, M., Habib, M. H., Alassmy, Y. A., Abduljawad, M. M., Alshamrani, K. M., & Sebakhy, K. O. (2022). Solid state NMR a powerful technique for investigating sustainable/renewable cellulose-based materials. *Polymers, 14*(5), 1049. https://doi.org/10.3390/polym14051049

El-shorbagy, A. M., El-badawy, S. M., & Gabr, A. R. (2019). Investigation of waste oils as rejuvenators of aged bitumen for sustainable pavement. *Construction and Building Materials, 220*, 228–237. https://doi.org/10.1016/j.conbuildmat.2019.05.180

Eskandarsefat, S., Hofko, B., Rossi, C. O., & Sangiorgi, C. (2019). Fundamental properties of bitumen binders containing novel cellulose-based poly-functional fibres. *Composites Part B: Engineering, 163*, 339–350.

Espinosa, E., Sánchez, R., Otero, R., Domínguez-Robles, J., & Rodríguez, A. (2017). A comparative study of the suitability of different cereal straws for lignocellulose nanofibers isolation. *International Journal of Biological Macromolecules, 103*, 990–999. https://doi.org/10.1016/j.ijbiomac.2017.05.156

Foston, M. (2014). Advances in solid-state NMR of cellulose. *Current Opinion in Biotechnology, 27*, 176–184. https://doi.org/10.1016/j.copbio.2014.02.002

French, A. D. (2014). Idealized powder diffraction patterns for cellulose polymorphs. *Cellulose, 21*(2), 885–896. https://doi.org/10.1007/s10570-013-0030-4

French, A. D., & Santiago Cintrón, M. (2013). Cellulose polymorphy, crystallite size, and the Segal crystallinity index. *Cellulose, 20*(1), 583–588. https://doi.org/10.1007/s10570-012-9833-y

Frone, A. N., Berlioz, S., Chailan, J.-F., & Panaitescu, D. M. (2013). Morphology and thermal properties of PLA-cellulose nanofibers composites. *Carbohydrate Polymers, 91*(1), 377–384.

García-Astrain, C., González, K., Gurrea, T., Guaresti, O., Algar, I., Eceiza, A., & Gabilondo, N. (2016). Maleimide-grafted cellulose nanocrystals as cross-linkers for bionanocomposite hydrogels. *Carbohydrate Polymers, 149*, 94–101. https://doi.org/10.1016/j.carbpol.2016.04.091

Glisin, D., Jovanovic, O., Stojanovic, G., Zivkovic, A., Stojanovic, D., Pavlovic, M., & Arsic, B. (2024). Synthesis of methyl 3,4-anhydro-6-bromo-2-o-tert-butyldimethyl-silyl-6-deoxy-a-d-allopyranoside from a-d-glucose. *Journal of the Serbian Chemical Society, 89*(9), 1123–1131. https://doi.org/10.2298/JSC230831049G

Goussé, C., Chanzy, H., Cerrada, M. L., & Fleury, E. (2004). Surface silylation of cellulose microfibrils: Preparation and rheological properties. *Polymer, 45*(5), 1569–1575. https://doi.org/10.1016/j.polymer.2003.12.028

Goussé, C., Chanzy, H., Excoffier, G., Soubeyrand, L., & Fleury, E. (2002). Stable suspensions of partially silylated cellulose whiskers dispersed in organic solvents. *Polymer, 43*(9), 2645–2651. https://doi.org/10.1016/S0032-3861(02)00051-4

Holding, A. J., Mäkelä, V., Tolonen, L., Sixta, H., Kilpeläinen, I., & King, A. W. T. (2016). Solution-state one- and two-dimensional NMR spectroscopy of high-molecular-weight cellulose. *ChemSusChem, 9*(8), 880–892. https://doi.org/10.1002/cssc.201501511

Horikawa, Y., Hirano, S., Mihashi, A., Kobayashi, Y., Zhai, S., & Sugiyama, J. (2019). Prediction of lignin contents from infrared spectroscopy: Chemical digestion and lignin/biomass ratios of Cryptomeria japonica. *Applied Biochemistry and Biotechnology, 188*(4), 1066–1076. https://doi.org/10.1007/s12010-019-02965-8

Jankauskait, V., Bal i naitien, A., Alexandrova, R., Bukuvien, N., & ukien, K. (2020). Effect of cellulose microfiber silylation procedures on the properties and antibacterial activity of polydimethylsiloxane. *Coatings, 10*(6), 567.

Jankauskaitė, V., Balčiūnaitienė, A., Alexandrova, R., Buškuvienė, N., & Žukienė, K. (2020). Effect of cellulose microfiber Silylation procedures on the properties and antibacterial activity of polydimethylsiloxane. *Coatings, 10*(6), 567. https://doi.org/10.3390/coatings10060567

Jing, M., Zhang, L., Fan, Z., Liu, X., Wang, Y., Liu, C., & Shen, C. (2022). Markedly improved hydrophobicity of cellulose film via a simple one-step aminosilane-assisted ball milling. *Carbohydrate Polymers, 275*, Article 118701. https://doi.org/10.1016/j.carbpol.2021.118701

Karnati, S. R., Oldham, D., Fini, E. H., & Zhang, L. (2020). Application of surface-modified silica nanoparticles with dual silane coupling agents in bitumen for performance enhancement. *Construction and Building Materials, 244*, Article 118324. https://doi.org/10.1016/j.conbuildmat.2020.118324

Khanjanzadeh, H., Behrooz, R., Bahramifar, N., Gindl-Altmutter, W., Bacher, M., Edler, M., & Griesser, T. (2018). Surface chemical functionalization of cellulose

nanocrystals by 3-aminopropyltriethoxysilane. *International Journal of Biological Macromolecules, 106*, 1288–1296. https://doi.org/10.1016/j.ijbiomac.2017.08.136
Kim, H., Youn, J. R., & Song, Y. S. (2018). Eco-friendly flame retardant nanocrystalline cellulose prepared via silylation. *Nanotechnology, 29*(45), Article 455702. https://doi.org/10.1088/1361-6528/aadc87
Kong, L., Sun, J., & Bao, Y. (2017). Preparation, characterization and tribological mechanism of nanofluids. *RSC Advances, 7*(21), 12599–12609. https://doi.org/10.1039/C6RA28243A
Lawandi, J., Rocheleau, S., & Moitessier, N. (2016). Regioselective acylation, alkylation, silylation and glycosylation of monosaccharides. *Tetrahedron, 72*(41), 6283–6319. https://doi.org/10.1016/j.tet.2016.08.019
Lee, J. H., Park, S. H., & Kim, S. H. (2020). Surface alkylation of cellulose nanocrystals to enhance their compatibility with polylactide. *Polymers, 12*(1), 178.
Li, M., Wu, Q., Moon, R. J., Hubbe, M. A., & Bortner, M. J. (2021). Rheological aspects of cellulose nanomaterials: Governing factors and emerging applications. *Advanced Materials, 33*(21). https://doi.org/10.1002/adma.202006052
Liu, D., Chen, X., Yue, Y., Chen, M., & Wu, Q. (2011). Structure and rheology of nanocrystalline cellulose. *Carbohydrate Polymers, 84*(1), 316–322. https://doi.org/10.1016/j.carbpol.2010.11.039
Lu, J., Askeland, P., & Drzal, L. T. (2008). Surface modification of microfibrillated cellulose for epoxy composite applications. *Polymer, 49*(5), 1285–1296.
Lv, J., Luo, T., Zou, D., & Dong, H. (2019). Using DMF as both a catalyst and Cosolvent for the Regioselective Silylation of polyols and diols. *European Journal of Organic Chemistry, 2019*(37), 6383–6395. https://doi.org/10.1002/ejoc.201901195
Martín-Alfonso, J. E., López-Beltrán, F., Valencia, C., & Franco, J. M. (2018). Effect of an alkali treatment on the development of cellulose pulp-based gel-like dispersions in vegetable oil for use as lubricants. *Tribology International, 123*, 329–336. https://doi.org/10.1016/j.triboint.2018.02.027
Martín-Alfonso, J. E., Martín-Alfonso, M. J., & Franco, J. M. (2020). Tunable rheological-tribological performance of "green" gel-like dispersions based on sepiolite and castor oil for lubricant applications. *Applied Clay Science, 192*, Article 105632. https://doi.org/10.1016/j.clay.2020.105632
Martín-Alfonso, J. E., Moreno, G., Valencia, C., Sánchez, M. C., Franco, J. M., & Gallegos, C. (2009). Influence of soap/polymer concentration ratio on the rheological properties of lithium lubricating greases modified with virgin LDPE. *Journal of Industrial and Engineering Chemistry, 15*(5), 687–693. https://doi.org/10.1016/j.jiec.2009.09.046
Martín-Alfonso, J. E., & Valencia, C. (2015). Tribological, rheological, and microstructural characterization of oleogels based on EVA copolymer and vegetables oils for lubricant applications. *Tribology International, 90*, 426–434.
Martín-Alfonso, J. E., Valencia, C., Arteaga, J. F., Díaz, M. J., & Franco, J. M. (2013). Design of lubricating grease formulations using recycled polypropylene from postconsumer films as thickener agent. *Journal of Applied Polymer Science, 127*(2), 1369–1376. https://doi.org/10.1002/app.37726
Martín-Alfonso, J. E., Valencia, C., Sánchez, M. C., Franco, J. M., & Gallegos, C. (2009). Rheological modification of lubricating greases with recycled polymers from different plastics waste. *Industrial & Engineering Chemistry Research, 48*(8), 4136–4144. https://doi.org/10.1021/ie801359g
Martín-Alfonso, J. E., Valencia, C., Sánchez, M. C., Franco, J. M., & Gallegos, C. (2011). Evaluation of different polyolefins as rheology modifier additives in lubricating grease formulations. *Materials Chemistry and Physics, 128*(3), 530–538. https://doi.org/10.1016/j.matchemphys.2011.03.046
Martín-Alfonso, M. A., Rubio-Valle, J. F., Hinestroza, J. P., & Martín-Alfonso, J. E. (2022). Impact of vegetable oil type on the rheological and Tribological behavior of montmorillonite-based Oleogels. *Gels, 8*(8), 504. https://doi.org/10.3390/gels8080504
Martínez-Boza, F., Partal, P., Conde, B., & Gallegos, C. (2000). Influence of temperature and composition on the linear viscoelastic properties of synthetic binders. *Energy & Fuels, 14*(1), 131–137. https://doi.org/10.1021/ef990072f
Md Salim, R., Asik, J., & Sarjadi, M. S. (2021). Chemical functional groups of extractives, cellulose and lignin extracted from native Leucaena leucocephala bark. *Wood Science and Technology, 55*(2), 295–313. https://doi.org/10.1007/s00226-020-01258-2
Mittal, A., Scott, G. M., Amidon, T. E., Kiemle, D. J., & Stipanovic, A. J. (2009). Quantitative analysis of sugars in wood hydrolyzates with 1H NMR during the autohydrolysis of hardwoods. *Bioresource Technology, 100*(24), 6398–6406. https://doi.org/10.1016/j.biortech.2009.06.107
Montplaisir, D., Daneault, C., & Chabot, B. (2008). Surface composition of grafted thermomechanical pulp through XPS measurement. *BioResources, 3*(4), 1118–1129. https://doi.org/10.15376/biores.3.4.1118-1129
Mormann, W., & Wagner, T. (2000). Silylation of cellulose with hexamethyldisilazane in liquid ammonia. *Carbohydrate Polymers, 43*(3), 257–262. https://doi.org/10.1016/S0144-8617(00)00173-9
Nouvel, C., Dubois, P., Dellacherie, E., & Six, J.-L. (2003). Silylation reaction of dextran: Effect of experimental conditions on Silylation yield, Regioselectivity, and chemical stability of Silylated Dextrans. *Biomacromolecules, 4*(5), 1443–1450. https://doi.org/10.1021/bm034119m
Pathan, A. K., Bond, J., & Gaskin, R. E. (2010). Sample preparation for SEM of plant surfaces. *Materials Today, 12*, 32–43. https://doi.org/10.1016/S1369-7021(10)70143-7
Patschinski, P., Zhang, C., & Zipse, H. (2014). The Lewis Base-catalyzed Silylation of alcohols—A mechanistic analysis. *The Journal of Organic Chemistry, 79*(17), 8348–8357. https://doi.org/10.1021/jo5016568
Patschinski, P., & Zipse, H. (2015). Leaving group effects on the selectivity of the silylation of alcohols: The reactivity–selectivity principle revisited. *Organic Letters, 17*(13), 3318–3321. https://doi.org/10.1021/acs.orglett.5b01536
Popescu, M.-C., Popescu, C.-M., Lisa, G., & Sakata, Y. (2011). Evaluation of morphological and chemical aspects of different wood species by spectroscopy and thermal methods. *Journal of Molecular Structure, 988*(1–3), 65–72. https://doi.org/10.1016/j.molstruc.2010.12.004
Qu, P., Zhou, Y., Zhang, X., Yao, S., & Zhang, L. (2012). Surface modification of cellulose nanofibrils for poly (lactic acid) composite application. *Journal of Applied Polymer Science, 125*(4), 3084–3091.
Rahnejat, H. (2010). *Tribology and dynamics of engine and powertrain: Fundamentals, applications and future trends*. Elsevier.
Ramírez, J. A.Á., Suriano, C. J., Cerrutti, P., & Foresti, M. L. (2014). Surface esterification of cellulose nanofibers by a simple organocatalytic methodology. *Carbohydrate Polymers, 114*, 416–423.
Rojas-Escudero, E., Alarcón-Jiménez, A. L., Elizalde-Galván, P., & Rojo-Callejas, F. (2004). Optimization of carbohydrate silylation for gas chromatography. *Journal of Chromatography A, 1027*(1–2), 117–120. https://doi.org/10.1016/j.chroma.2003.10.131
Ross-Murphy, S. B. (1995). Rheological characterisation of GELS1. *Journal of Texture Studies, 26*(4), 391–400. https://doi.org/10.1111/j.1745-4603.1995.tb00979.x
Sain, M., & Panthapulakkal, S. (2006). Bioprocess preparation of wheat straw fibers and their characterization. *Industrial Crops and Products, 23*(1), 1–8. https://doi.org/10.1016/j.indcrop.2005.01.006
Saleem, M. (2022). Possibility of utilizing agriculture biomass as a renewable and sustainable future energy source. *Heliyon, 8*(2), Article e08905. https://doi.org/10.1016/j.heliyon.2022.e08905
Sayadi, S., & Brouillette, F. (2024). Silylation of phosphorylated cellulosic fibers with an aminosilane. *Carbohydrate Polymers, 343*, Article 122500. https://doi.org/10.1016/j.carbpol.2024.122500
Segal, L., Creely, J. J., Martin, A. E., & Conrad, C. M. (1959). An empirical method for estimating the degree of crystallinity of native cellulose using the X-ray diffractometer. *Textile Research Journal, 29*(10), 786–794. https://doi.org/10.1177/004051755902901003
Shafiei-Sabet, S., Hamad, W. Y., & Hatzikiriakos, S. G. (2012). Rheology of Nanocrystalline cellulose aqueous suspensions. *Langmuir, 28*(49), 17124–17133. https://doi.org/10.1021/la303380v
Shafiei-Sabet, S., Martinez, M., & Olson, J. (2016). Shear rheology of micro-fibrillar cellulose aqueous suspensions. *Cellulose, 23*(5), 2943–2953. https://doi.org/10.1007/s10570-016-1040-9
Shariati, S., Aldagari, S., & Fini, E. H. (2023). Bio-modifier: A sustainable suturing technology at the bitumen–aggregate interface. *ACS Sustainable Chemistry & Engineering, 11*(24), 8908–8915. https://doi.org/10.1021/acssuschemeng.3c01001
Souguir, Z., Dupont, A.-L., Fatyeyeva, K., Mortha, G., Cheradame, H., Ipert, S., & Lavédrine, B. (2012). Strengthening of degraded cellulosic material using a diamine alkylalkoxysilane. *RSC Advances, 2*(19), 7470. https://doi.org/10.1039/c2ra20957h
Tao, P., Zhang, Y., Wu, Z., Liao, X., & Nie, S. (2019). Enzymatic pretreatment for cellulose nanofibrils isolation from bagasse pulp: Transition of cellulose crystal structure. *Carbohydrate Polymers, 214*, 1–7. https://doi.org/10.1016/j.carbpol.2019.03.012
Theander, O., & Westerlund, E. A. (1986). Studies on dietary fiber. 3. Improved procedures for analysis of dietary fiber. *Journal of Agricultural and Food Chemistry, 34*(2), 330–336.
Tingaut, P., Hauert, R., & Zimmermann, T. (2011). Highly efficient and straightforward functionalization of cellulose films with thiol-ene click chemistry. *Journal of Materials Chemistry, 21*(40), Article 16066. https://doi.org/10.1039/c1jm11620g
Trejo-Cáceres, M., Sánchez, M. C., & Martín-Alfonso, J. E. (2024). Assessment of the acetylation process of wheat straw pulp as sustainable rheological modifier for non-polar fluids. *Cellulose, 31*(4), 2063–2078. https://doi.org/10.1007/s10570-024-05750-x
Tursi, A., Beneduci, A., Chidichimo, F., De Vietro, N., & Chidichimo, G. (2018). Remediation of hydrocarbons polluted water by hydrophobic functionalized cellulose. *Chemosphere, 201*, 530–539.
Wei, D. W., Wei, H., Gauthier, A. C., Song, J., Jin, Y., & Xiao, H. (2020). Superhydrophobic modification of cellulose and cotton textiles: Methodologies and applications. *Journal of Bioresources and Bioproducts, 5*(1), 1–15. https://doi.org/10.1016/j.jobab.2020.03.001
Weldu, W. D., & Wang, C.-C. (2021). Selective acetylation of non-anomeric groups of per-O -Trimethylsilylated sugars. *The Journal of Organic Chemistry, 86*(7), 5336–5344. https://doi.org/10.1021/acs.joc.0c02813
Yuan, T., Zeng, J., Wang, B., Cheng, Z., & Chen, K. (2021). Cellulosic fiber: Mechanical fibrillation-morphology-rheology relationships. *Cellulose, 28*(12), 7651–7662. https://doi.org/10.1007/s10570-021-04034-y
Zhang, B., Xu, Y., Gao, F., Shi, P., Xu, B., & Wu, Y. (2011). Sliding friction and wear behaviors of surface-coated natural serpentine mineral powders as lubricant additive. *Applied Surface Science, 257*(7), 2540–2549. https://doi.org/10.1016/j.apsusc.2010.10.019
Zhang, B.-S., Xu, B.-S., Xu, Y., Gao, F., Shi, P.-J., & Wu, Y.-X. (2011). CU nanoparticles effect on the tribological properties of hydrosilicate powders as lubricant additive for steel–steel contacts. *Tribology International, 44*(7–8), 878–886. https://doi.org/10.1016/j.triboint.2011.03.002
Zhang, M., & James, S. P. (2005). Silylation of hyaluronan to improve hydrophobicity and reactivity for improved processing and derivatization. *Polymer, 46*(11), 3639–3648. https://doi.org/10.1016/j.polymer.2005.03.022
Zhang, Z., Sèbe, G., Rentsch, D., Zimmermann, T., & Tingaut, P. (2014). Ultralightweight and flexible Silylated Nanocellulose sponges for the selective removal of oil from

water. *Chemistry of Materials, 26*(8), 2659–2668. https://doi.org/10.1021/cm5004164

Zhang, Z., Tingaut, P., Rentsch, D., Zimmermann, T., & Sèbe, G. (2015). Controlled Silylation of Nanofibrillated cellulose in water: Reinforcement of a model polydimethylsiloxane network. *ChemSusChem, 8*(16), 2681–2690. https://doi.org/10.1002/cssc.201500525

Zhou, T., Kabir, S. F., Cao, L., & Fini, E. H. (2021). Effects of ultraviolet exposure on physicochemical and mechanical properties of bio-modified rubberized bitumen: Sustainability promotion and resource conservation. *Resources, Conservation and Recycling, 171*, Article 105626. https://doi.org/10.1016/j.resconrec.2021.105626